

Heat and mass transfer analysis of nonmiscible couple stress fluid in a porous saturated channel

Pramod Kumar Yadav*, Ankit Kumar*[‡] and Ali J. Chamkha[†]

**Department of Mathematics,
Motilal Nehru National Institute of Technology Allahabad,
Prayagraj 211004, Uttar Pradesh, India*

*†Faculty of Engineering,
Kuwait College of Science and Technology,
Doha District, 35004 Kuwait*

‡ankitkumar@mnnit.ac.in

Received 24 November 2022

Revised 17 February 2023

Accepted 25 February 2023

Published 17 July 2023

The present flow problem analyzes the impact of radiative heat and mass transfer with inclined magnetic field on thermal exchange and entropy production of two immiscible nature of electrically conducting couple stress fluid in a static porous saturated conduit. In this model, the lower and upper porous regions of the rectangular channel are occupied by two different types of couple stress fluids. The static horizontal parallel plates of the porous duct are completely isothermal and the flow of immiscible fluid through the porous duct develops because of a constant pressure gradient at the entry zone of the duct. The Brinkman model is utilized in the modeling of fluid flow through porous saturated domain and Rosseland's approximation is utilized to compute the radiative thermal exchange effect on nonmiscible couple stress fluid. In this work, authors have analyzed the effect of various thermo-physical parameters such as the Hartmann number (Ha), permeability parameter (Da), Schmidt number (Sc), Soret number (Sr) and couple stress parameter ($s_i, i = 1, 2$) on the entropy generation characteristics, Bejan number distribution, thermal behavior, concentration distribution and flow characteristics of immiscible couple stress fluid which passes through the porous channel. The parameters Ha, Da, s_i , Sc, Sr correspond to magnetic field effect, permeability of porous media, couple stress, mass diffusion and thermal diffusion, respectively. The most significant findings of this research work are as follows:

- In a porous saturated channel, the immiscible couple stress fluid velocity, entropy production number and thermal profile get enhanced on increasing the couple stress parameter.
- On increasing the Hartmann number and decreasing the permeability of porous region, the thermal properties and entropy production number both decrease.
- The couple stress fluid's concentration field and Bejan number distribution get decreased on enhancing Soret number Sr and Schmidt number Sc.
- The entropy generation near the wall of the channel rapidly increases on increasing the Schmidt number and Soret number.

[‡]Corresponding author.

The emerging finding of this research work exhibits excellent agreement with previously published work. This research work can be utilized in food processing, petroleum products and chemical process.

Keywords: Couple stress fluid; heat and mass transfer; immiscible fluid; porous media; entropy generation number.

PACS numbers: 47.56.+r, 47.60.+i, 47.65.-d, 47.15.G-, 47.15.-x.

Nomenclature

Physical constants

$(S_i)_G$: Volumetric entropy production rate of the phases [J/kg K]

B : Magnetic field [T]

B_0 : Magnetic field strength

Be : Bejan number

Br : Brinkman number

C_i : Concentration of the phases [kg m^{-3}]

D_{m_i} : Mass diffusivity of the phases [$\text{m}^2 \text{s}^{-1}$]

Da : Permeability parameter

E : Electric field [V m^{-1}]

h : Characteristics distance [m]

Ha : Hartmann number

J : Current density [A m^{-2}]

K_i : Porous medium permeability of the phases [m^2]

k_i : Thermal conductivity of the phases [$\text{W m}^{-1} \text{K}^{-1}$]

k_{T_i} : Thermal diffusion ratio of the phases

n_i : Dimensionless concentration of the phases

Nr : Radiation parameter

Ns_i : Dimensionless entropy production number of the phases

P : Pressure [N m^{-2}]

p_i : Irreversibility distribution ratio of the phases

q_r : Radiative heat flux [W m^{-2}]

Re : Reynolds number

s_i : Couple stress parameter of the phases

$S_{G,C}$: Characteristics rate of entropy production

Sc : Schmidt number

Sr : Soret number

T : Temperature [K]

T_0 : Reference temperature

T_i : Temperature of the phases [K]

T_m : Mean temperature [K]

U_0 : Characteristics velocity [m s^{-1}]

u_i : Dimensional velocity [m s^{-1}]
 x, y : Dimensional coordinates [m]
 x^*, y^* : Dimensionless coordinates [m]

Greeks Letter

k^* : Mean absorption coefficient
 ΔT : Temperature difference
 η_i : Viscosity coefficients of couple stress fluid for the phases
 Λ : Diffusive constant parameter
 λ : Inclination angle of the magnetic field
 μ_i : Dynamic viscosities of the phases [N s m^{-2}]
 Ω : Dimensionless temperature ratio
 π : Dimensionless concentration ratio
 ρ : Density [Kg m^{-3}]
 σ^* : Stefan–Boltzmann constant [$\text{W m}^{-2} \text{K}^{-4}$]
 σ_i : Electrical conductivity of the phases [Ω/m]
 θ_i : Dimensionless temperatures of the phases
 n_η : Couple stress parameter ratio
 n_μ : Viscosity ratio
 n_σ : Electrical conductivity ratio
 n_D : Mass diffusivity ratio
 n_K : Permeability ratio
 n_k : Thermal conductivity ratio
 n_R : Ideal gas constant ratio

Subscripts

gen : Generation
 i : For Region-1, $i = 1$, for Region-2, $i = 2$

1. Introduction

The study of magnetohydrodynamics (MHD), thermal exchange and fluid flow processes has been the central part of investigation for various researchers and scientists due to their enormous roles in various sectors of industries and engineering communities. Due to dynamic thermo-physical properties, this field of research can be employed for a wide range of practical applications in engineering such as electrostatic precipitation, the petroleum industry, aerodynamic heating, power generators and polymer technology. The subject of nonmiscible fluid with MHD has great importance in the area of biomedical science such as reduction of bleeding

during surgeries, cancer treatment, transport of drugs, blood flow in arteries and crude oil extraction. Several comprehensive studies have recently been published by utilizing the MHD flow and convective thermal exchange of immiscible fluid through different geometries and under different boundary conditions. Adesanya and Makinde¹ investigated the thermal exchange impact on the magnetized flow of non-Newtonian couple stress fluid within a vertical porous conduit. They employed the Adomian decomposition technique for evaluating the analytical solutions of thermal exchange and flow velocity. Abbas *et al.*² analyzed the hydromagnetic flow distribution and heat exchange of nonmiscible nature of couple stress fluid within an inclined duct. Ramesh³ addressed the heat, mass and magnetic field effect on peristaltic phenomena of a couple stress fluid in an inclined asymmetric porous saturated duct. Umavathi *et al.*⁴ studied the fully developed, laminar flow and thermal exchange of couple stress fluid inside a horizontal conduit bounded by two viscous fluid layers. Kamisli and Öztöp⁵ estimated the impact of pressure gradient on entropy production of incompressible and nonmiscible flows of viscous fluids within a horizontal thin slit. On the basis of a uniform heat sink and source, Kumar *et al.*⁶ analyzed the flow of a ferromagnetic viscous fluid with thermophoretic molecular diffusion over a stretching cylinder. Kumar *et al.*⁷ analyzed the heat and mass transport analysis on the flow of an incompressible Casson fluid with thermophoretic molecular diffusion along a horizontal thin moving needle. The heat exchange analysis in the MHD three-dimensional unsteady flow of non-Newtonian nanofluid is studied by Kumar *et al.*⁸ Asogwa *et al.*⁹ talked about the Lorentz force and heat sink phenomena on the flow of Casson fluid over an inclined Riga plate under the influence of Dufour and Soret. In a heterogeneous Brinkman porous layer with a uniformly dispersed internal source of heat and a vertical magnetic field, Ravisha *et al.*¹⁰ proposed the linear theory for the ferromagnetic convective flow. Abdelsalam and Zaher¹¹ did a theoretical study on the influence of electroosmotic pressures on sperm moving in the cervical canal. Alsharif *et al.*¹² theoretically examined copper and titanium low-dense mixes of two spherical nanoparticles in unsteady, incompressible and electroosmotic flow (EOF) of a fractional second-grade fluid. Abdelsalam *et al.*¹³ investigated the effects of laser light, electromagnetic field, chemical processes and electro-osmosis flow of hybridized non-Newtonian fluid along a sinusoidal channel. The impacts of nonlinear density temperature and nonuniform source/sink of heat on three-dimensional Maxwell nanofluid flow across a stretching sheet were investigated numerically by Thumma *et al.*¹⁴

In modern times, the comprehensive study of non-Newtonian fluids has gained crucial importance in various fields of research because of its extensive applications in engineering mechanisms, biological and physiological science, and industrial manufacturing processes. Significantly, such fluids are utilized in chemical and nuclear industries, fiber technology, food processing, oil reservoir engineering and pharmaceutical companies. The constitutive equations of non-Newtonian fluids are nonlinear in nature, so it is the most challenging work for researchers, scientists and the engineering community. Keeping such distinct features in mind, many

researchers and scientists follow the modeling of non-Newtonian fluids under various flow situations and geometric configurations. Due to their complex nature, the rheological characteristics of non-Newtonian fluids are determined by their constitutive equations. Many researchers and scientists have developed different non-Newtonian fluid models and their constitutive equations under various flow situations and conditions. The classical theory of couple stress fluid was introduced by Stokes.^{15,16} Couple stress fluid possesses the effects of polarity in the form of body couples and couple stress. Ariman and Cakmak¹⁷ estimated the various roles of couple stress fluid under different flow geometries and flow situations, and they compared these results with micropolar fluids. Mekheimer¹⁸ estimated the peristaltic nature of couple stress fluid in a conduit with approximation of long wavelength. Srinivasacharya *et al.*¹⁹ analyzed the thermal characteristics and flow behavior of a couple stress fluid within a porous conduit with contracting and expanding walls. Khan *et al.*²⁰ investigated the Maxwell bio-convective nanofluid flow via an exponentially extending curved surface under convective boundary conditions. Raza *et al.*²¹ examined the impact of hydrodynamics on the radiative Sutterby nanofluid flow across a stretchy cylinder.

The design and optimization techniques of various thermo-fluidic devices have been prepared by using the thermodynamic second law. It determines the irreversible losses that arise because of thermal exchange and fluid flow processes in the form of entropy production rate. Entropy production is a thermodynamic variable which is used to quantify the irreversibility distribution in various thermal systems. The thermodynamic second law is used to select the appropriate design techniques and optimum conditions by minimizing the total entropy generation rates. Moreover, this method of minimization is defined as entropy generation minimization (EGM) which measures the performance and working capacity of thermal devices and engineering technologies. The topic of entropy production provides a set of operating conditions and design parameters that enhance the performance of thermal power systems such as heat pumps, energy storage systems, cooling of electronic devices, heat exchangers and so on. It is well understood that distinct factors such as porous media, magnetic fields, viscous dissipation, thermal radiation, heat and mass exchange are responsible for the generation of entropy in thermal processes. The concept, working procedure and minimization of entropy production are addressed by Bejan *et al.*^{22,23} Bejan^{24,25} also introduced the thermal exchange process in conduit flow, peristaltic transportation, boundary layer flow and flow through various portions of the conduit using the concept of EGM. Sridhar *et al.*²⁶ examined the effects of diamond and copper nanoparticles on the peristaltic phenomenon of couple stress nanofluid controlled by the electro-magneto-hydrodynamic process in a vertical microchannel. Faizan *et al.*²⁷ used Cattaneo-Christov double diffusion model to investigate the entropy production of a Sutterby nanofluid on a Riga plate. Makinde and Eegunjobi²⁸ studied the entropy generation characteristics of incompressible couple stress fluid inside a vertical porous saturated duct. Srinivas *et al.*²⁹ discussed the thermodynamic second and first law analysis of

nonmiscible couple stress fluid within a horizontal rectangular duct sandwiched by two porous beds. Nagaraju *et al.*³⁰ analyzed the production of entropy in an electrically conducting and magnetized couple stress fluid flow within a porous annulus bounded by two concentric cylinders. Aksoy³¹ investigated the thermal exchange, entropy production and flow characteristics of a couple stress fluids within a parallel plate channel with constant thermal flux. Entropy production for the reactive nature of couple stress fluid inside a porous conduit was analyzed by Adesanya *et al.*³² Srinivas *et al.*³³ described the influence of radiative thermal exchange on entropy production of two-layered immiscible nature of couple stress fluid inside a rectangular pipe. The flow of magnetized and nonmiscible couple stress fluid within a horizontal conduit was analyzed by Murthy and Srinivas.³⁴ The entropy analysis due to thermal exchange with viscous dissipation is also useful in electric as well as solar power generation. Jangili *et al.*³⁵ analyzed the influence of radiative thermal exchange on convective heat transformation and entropy production analysis of steady-state micropolar fluid within a vertical porous conduit. Arpaci^{36,37} discussed the entropy analysis because of radiative thermal exchange in various flow situations. Yadav and Kumar³⁸ investigated the impact of oriented magnetic field on entropy generation characteristics of two-layered flow of immiscible micropolar and Newtonian fluid in a parallel plate conduit. Yadav *et al.*³⁹ examined the influence of different porosity on entropy generation characteristics of two MHD and radiative flow of immiscible micropolar and Newtonian fluid in a porous saturated medium. Yadav *et al.*⁴⁰ talked about the effects of thermal radiation and magnetic fields on the Bejan number profile, thermal properties, flow velocity and entropy production of micropolar and Newtonian viscous fluid inside a channel. Jamshed *et al.*⁴¹ studied the nanofluid flow and thermal exchange process by exposing it to a slippery surface under the influence of thermal radiation, heat source, viscous dissipation and porous media. Alhadhrami *et al.*⁴² analyzed the impact of local thermal nonequilibrium on the flow and thermal exchange of non-Newtonian Casson fluid in a porous saturated medium. In a rectangular chamber filled with water hybrid nanofluids and attached to a wall made of a phase change material (PCM), Al-Maliki *et al.*⁴³ conducted an experimental study to examine the natural convective thermal exchange. Sarris *et al.*⁴⁴ carried out a numerical analysis of the thermal exchange and buoyancy-driven flow in a two-dimensional open container with localized below-surface heating and cooling.

Many researchers and scientists are studying the entropy generation analysis of immiscible types of non-Newtonian fluids through porous media because of their crucial roles in numerous emerging areas of science and technology. This entropy production analysis is also required to improve the working capacity of various scientific devices by minimizing entropy generation. In this work, authors investigated the influence of radiative heat transfer, mass transfer and inclined magnetic field on entropy generation characteristics of two immiscible type of incompressible couple stress fluid in a porous saturated domain. The analyses of concentration profile with entropy production of immiscible fluid have enormous practical

applications in engineering laboratories, space center and thermal power plants. Hence, this study can be utilized in food processing, hydrometallurgical industries, polymer production, chemical process and manufacturing of ceramics. It is essential to study the importance of porous saturated channels which may be used for sound absorption, heat insulation and electrical applications.

Research gaps: To the best of the authors' knowledge and previously published research work which underlines the application and importance of heat exchange and mass exchange on entropy production analysis of two different natures of MHD and radiative nonmiscible couple stress fluid in a porous channel has been analyzed yet. The previously published kinds of the literature also conclude that no study highlights the Bejan number distribution due to mass exchange of nonmiscible couple stress fluid in a porous medium. These important results motivate the authors to work in this area to present some new findings along with the existing results.

Novelty: In present flow problem, the main emphasize is given on creation of entropy due to mass transfer of immiscible type of couple stress fluid in porous saturated channel. Here, authors have analyzed the influence of radiative heat exchange, mass exchange, oriented magnetic field and radiative heat transfer on entropy generation of two-phase immiscible nature of couple stress fluid within a porous saturated duct. The impact of various thermo-physical parameters such as permeability parameter, couple stress parameter, radiation parameter, Schmidt number, inclination angle parameter, Soret number and Hartmann number on the entropy generation number, temperature field, concentration field, Bejan number distribution and flow velocity of immiscible couple stress fluid has been graphically analyzed. In this work, the concentration species of immiscible couple stress fluid is also analyzed graphically and discussed in detail. On the basis of past published research work, authors noticed that no such type of study is performed which analyzed the significance of porous material on heat, mass exchange and concentration of two nonmiscible type of couple stress fluid in porous channel. This study may be used in various medical treatments and biomedical engineering such as in the thermal therapeutic process.

2. Governing Flow and Heat Transfer Equations for Immiscible Type of Couple Stress Fluid in a Porous Saturated Medium

The analysis of electrically conducting nonmiscible nature of couple stress fluid flow through a porous region in presence of radiative heat transfer and oriented magnetic field had numerous applications in geophysical and engineering technologies such as thermal insulation, drying of porous substances, cooling of electronic devices and nuclear reactors. The governing system of conservation equations for the flow of couple stress fluid is designated by energy equations, continuity equations together with conservation of momentum equation, which are addressed by Stokes^{15,16} and takes the form as

Continuity equation^{15,16}:

$$\frac{\partial \rho}{\partial t} + \nabla \cdot (\rho \mathbf{v}) = 0. \quad (1)$$

The scalar quantity ρ and vector quantity \mathbf{v} represent the fluid density and flow velocity of couple stress fluid, respectively.

Momentum equation^{15,16}:

$$\begin{aligned} \rho \frac{D\mathbf{v}}{Dt} = & -\nabla P + \mu \nabla \times \nabla \times \mathbf{v} + (\lambda_1 + 2\mu) \nabla (\nabla \cdot \mathbf{v}) - \eta \nabla \\ & \times \nabla \times \nabla \times \mathbf{v} + \mathbf{J} \times \mathbf{B} - \frac{\mu}{K} \mathbf{v}. \end{aligned} \quad (2)$$

The fluid pressure is denoted by scalar quantity P . The material constants (viscosity coefficients) are denoted by symbols (λ_1, μ) and viscosity coefficients of couple stress are denoted by symbols η and η' which satisfy the constraints $\eta \geq 0$; $\mu \geq 0$; $|\eta'| \leq \eta$; $3\lambda_1 + 2\mu \geq 0$. The second last term $\mathbf{J} \times \mathbf{B}$ in Eq. (2) represents the Lorentzian body force in which \mathbf{J} depicts the current density, which produces in the flow field because of existence of magnetic field \mathbf{B} .

Ohm's law in generalized form can be expressed as⁴⁵

$$\mathbf{J} = \sigma(\mathbf{E} + \mathbf{v} \times \mathbf{B}). \quad (3)$$

The vector quantity \mathbf{E} denotes the electric field and scalar quantity σ depicts the electrical conductivity of nonmiscible couple stress fluid. Since the electric field is not considered in the present problem, the electric current density \mathbf{J} takes the following form:

$$\mathbf{J} = \sigma(\mathbf{v} \times \mathbf{B}). \quad (4)$$

In 1856, Darcy,⁴⁶ a French engineer, performed a number of experiments in which he analyzed the flow of water in an vertical conduit of sand. He observed a proportional relation between the applied pressure gradient and flow rate of water which takes the following form:

$$\mathbf{v} = \frac{-K}{\mu} \nabla P. \quad (5)$$

Here, K and μ are, respectively, the permeability parameter and viscosity of fluid.

Some other flows that allow to transport the fluid through high porous material do not obey the Darcy's law. In 1947, Brinkman modifies the equation of Darcy's law by adding the term $\mu \nabla^2 \mathbf{v}$ to Darcy's law which is given as follows⁴⁷:

$$\mathbf{v} = \frac{-K}{\mu} \nabla P + \mu \nabla^2 \mathbf{v}. \quad (6)$$

Thermal energy equation^{15,16}:

$$\rho \frac{DE}{Dt} = \Phi + k \nabla^2 T + \frac{J^2}{\sigma} + \frac{\mu}{K} \mathbf{v}^2 - \nabla \cdot q_r, \quad (7)$$

where

$$\Phi = \mu [(\nabla \mathbf{v}) : (\nabla \mathbf{v})^T + (\nabla \mathbf{v}) : (\nabla \mathbf{v})] + 4\eta [(\nabla \omega) : (\nabla \omega)^T] + 4\eta' [(\nabla \omega) : (\nabla \omega)^T]. \quad (8)$$

The conservative laws of mass balance, momentum and energy balance equation are represented by Eqs. (1), (2) and (7), respectively. The vectorial quantity $\omega = \frac{1}{2}(\nabla \times \mathbf{v})$ denotes the rotational motion of couple stress fluid particles. In thermal energy equation, the notation Φ is used for mechanical energy per unit mass which is also known as dissipation function. The last term $\nabla \cdot q_r$ of Eq. (7) addressed the radiative heat flux of couple stress fluid flowing in the conduit.

Concentration equation⁴⁸:

$$\frac{DC}{Dt} = D_m \nabla^2 C + \frac{D_m k_T}{T_m} \nabla^2 T, \quad (9)$$

where C denotes the concentration, D_m represents the mass diffusivity coefficient, k_T stands for thermal diffusion ratio and T_m symbolized the mean temperature of the couple stress fluid.

The radiative thermal flux factor in the above equation can be approximated by Rosseland's diffusion approximation which takes the following form^{49,50}:

$$q_r = -\frac{4}{3} \frac{\sigma^*}{k^*} \frac{dT^4}{dy}. \quad (10)$$

Here, σ^* depicts the Stefan–Boltzmann constant and k^* denotes the mean absorption coefficient. According to flow circumstances, when the differences of temperature within fluid medium are sufficiently small, we may employ the Taylor series expansion for the temperature T with respect to reference temperature T_0 , i.e.,

$$T^4 = T_0^4 + 4T_0^3(T - T_0) + 6T_0^2(T - T_0)^2 + \dots \quad (11)$$

In the above expression, we consider only first degree term and remove the remaining terms:

$$T^4 = 4T_0^3 T - 3T_0^4. \quad (12)$$

In order to obtain the value of radiative thermal flux, we differentiated Eq. (10) with respect to y and uses Eq. (12), hence we obtain⁵¹

$$\frac{dq_r}{dy} = -\frac{16\sigma^* T_0^3}{3k^*} \frac{d^2 T}{dy^2}. \quad (13)$$

3. Mathematical Model and Solution of the Proposed Problem

3.1. Mathematical model

The problem of the simultaneous flow of nonmiscible fluids through pipe/conduit is of great practical application in industrial processes where two or more immiscible fluids take place simultaneously in the same pipe or channel. There are many more areas where the flow of two immiscible fluids occurs in the same channel. The entropy analysis of immiscible fluids flowing through pipe/conduit is also an essential need to think about the working capacity of thermal technologies in the form of conservation of energy. Therefore, the aim of our analysis is to further reduce the entropy production and achieve the best design of thermal devices when two couple stress fluids take place through the porous channel.

In the considered flow problem, two different types of electrically conducting nonmiscible couple stress fluid flow inside a rectangular channel which is built of two parallel plates and filled with two distinct non-Darcian porous materials whose permeabilities are different (Fig. 1). The flow of two nonmiscible, incompressible couple stress fluid is laminar, unidirectional and in steady state. The X - and Z -directions are the directions in which the channel's plates stretch, and the Y -direction is seen as normal by them. The flow regime is developed along the x -axis due to the applied constant pressure gradient. An oriented constant magnetic field B_0 is applied at an angle θ with the normal direction of the flow domain. The electric field and the induced magnetic field are not prescribed in the considered work and the characteristics of nonmiscible fluid are considered constant in nature. In the flow geometry, the bottom and upper walls of the conduit are situated at a distance of $2h$ apart, and it is assumed that the height of the conduit is sufficiently smaller than its length. Due to nonmiscibility, both the couple stress fluids cannot penetrate each other. The flow properties of couple stress fluid flowing in upper porous zone ($0 \leq y \leq h$) are taken as viscosity μ_2 , electrical conductivity σ_2 , flow velocity u_2 , thermal conductivity k_2 , permeability K_2 , thermal characteristics T_2 , concentration field C_2 , mass diffusivity coefficient D_{m_2} and thermal diffusion ratio k_{T_2} however, these flow properties for lower porous region ($-h \leq y \leq 0$) are taken as viscosity μ_1 ,

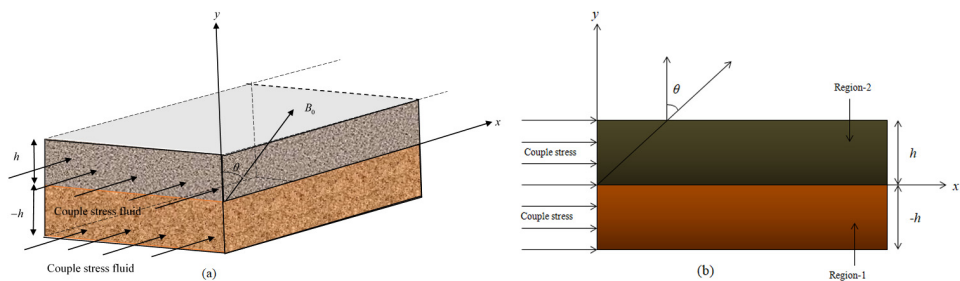


Fig. 1. (Color online) Schematic geometry of the physical problem.

flow velocity u_1 , electrical conductivity σ_1 , thermal conductivity k_1 , permeability K_1 and thermal characteristics T_1 , concentration field C_1 , mass diffusivity coefficient D_{m_1} and thermal diffusion ratio k_{T_1} .

For the modeling of the present problem, authors employed the following assumptions and conditions:

- The flow regime of nonmiscible couple stress fluid is unidirectional, laminar, axis symmetric, steady, viscous and incompressible.
- The transport characteristics of nonmiscible fluid are constant.
- The porous substances packed in a rectangular pipe are homogeneous and isotropic.
- A homogenous magnetic field is applied in the y -direction which is perpendicular to the flow direction.
- The flow is maintained via a continuous pressure gradient.
- The only body force operating on the fluid is the Lorentz force ($J \times B$).
- The isothermal walls of the channel are kept stationary.

The flow equations of radiative, viscous, incompressible, magnetized and steady-state flow regime of couple stress fluid within the lower porous zone of the rectangular porous pipe under the above assumptions are prescribed by Brinkman momentum, thermal energy equation and equation of continuity, which are as follows:

Continuity equation^{33,34}:

$$\nabla \cdot \mathbf{v}_1 = 0. \quad (14)$$

Momentum equation^{33,34}:

We consider the pressurized flow of couple stress fluid between two stationary parallel plates that are kept at 2 h apart and flow is assumed as incompressible, unidirectional, steady and laminar. Thus, the term on the left-hand side of Eq. (2) which is responsible for unsteady flow and the third term on the right-hand side of Eq. (2), because of continuity equation (1), should not be considered in the momentum equation (2).

Therefore, the momentum equation (2) under the considered assumption of the problem will become as

$$-\nabla P + \mu_1 \nabla \times \nabla \times \mathbf{v}_1 - \eta_1 \nabla \times \nabla \times \nabla \times \nabla \times \mathbf{v}_1 + J \times B - \frac{\mu_1}{K_1} \mathbf{v}_1 = 0. \quad (15)$$

The last term of Eq. (1) describes the flow of fluid through porous media and it comes from Darcy's law.

Energy equation^{33,34}:

Under the considered assumptions of the model, the energy equation (7) that underlines thermal analysis and determines how temperatures are distributed

between parallel plates will become as

$$k_1 \nabla^2 T_1 + \mu_1 [(\nabla \mathbf{v}_1) : (\nabla \mathbf{v}_1)^T + (\nabla \mathbf{v}_1) : (\nabla \mathbf{v}_1)] + 4\eta_1 [(\nabla \omega) : (\nabla \omega)^T] + 4\eta'_1 \times [(\nabla \omega) : (\nabla \omega)^T] + \frac{J^2}{\sigma} + \frac{\mu_1}{K_1} \mathbf{v}_1^2 - \nabla \cdot \mathbf{q}_r = 0. \quad (16)$$

The second, third and fourth components in Eq. (16) represent the contribution of viscous dissipation associated with Newtonian and couple stress effects.

Concentration equation⁴⁸:

The mass concentration equation for steady couple stress fluid flow in a porous saturated medium is given by

$$D_{m_1} \nabla^2 C_1 + \frac{D_{m_1} k_{T_1}}{T_m} \nabla^2 T_1 = 0. \quad (17)$$

The flow equations of radiative, viscous, incompressible, magnetized and steady-state flow regime of couple stress fluid within the upper porous zone of the rectangular porous pipe under the above assumptions are prescribed by Brinkman momentum, thermal energy equation and equation of continuity, which are as follows:

Continuity equation^{33,34}:

$$\nabla \cdot \mathbf{v}_2 = 0. \quad (18)$$

Momentum equation^{33,34}:

$$-\nabla P + \mu_2 \nabla \times \nabla \times \mathbf{v}_2 - \eta_2 \nabla \times \nabla \times \nabla \times \nabla \times \mathbf{v}_2 + J \times B - \frac{\mu_2}{K_2} \mathbf{v}_2 = 0. \quad (19)$$

Energy equation^{33,34}:

$$k_2 \nabla^2 T_2 + \mu_2 [(\nabla \mathbf{v}_2) : (\nabla \mathbf{v}_2)^T + (\nabla \mathbf{v}_2) : (\nabla \mathbf{v}_2)] + 4\eta_2 [(\nabla \omega) : (\nabla \omega)^T] + 4\eta'_2 \times [(\nabla \omega) : (\nabla \omega)^T] + \frac{J^2}{\sigma} + \frac{\mu_2}{K_2} \mathbf{v}_2^2 - \nabla \cdot \mathbf{q}_r = 0. \quad (20)$$

Concentration equation⁴⁸:

$$D_{m_2} \nabla^2 C_2 + \frac{D_{m_2} k_{T_2}}{T_m} \nabla^2 T_2 = 0. \quad (21)$$

The flow velocity components of couple stress fluid in lower porous zone of the duct under the above assumptions are considered as $\mathbf{v}_1 = (u_1, 0, 0)$. Due to existence of continuity equation for incompressible nature of fluid in a fully developed flow regime, the x -axis component of flow velocity will become the function of y only, i.e., $u_1 = u_1(y)$ and its y -directional velocity component vanishes.

Within the framework of above criteria, the governing flow equations for radiative, magnetized, viscous and incompressible flow regime of couple stress fluid in

bottom porous zone of the duct will become as

Conservation of linear momentum^{33,34}:

$$\frac{dp}{dx} = \mu_1 \frac{d^2 u_1}{dy^2} - \eta_1 \frac{d^4 u_1}{dy^4} - \sigma_1 B_0^2 \lambda^2 u_1 - \frac{\mu_1}{K_1} u_1. \quad (22)$$

Conservation of energy^{33,34}:

$$\left(k_1 + \frac{16\sigma^* T_0^3}{3k^*} \right) \frac{d^2 T_1}{dy^2} + \mu_1 \left(\frac{du_1}{dy} \right)^2 + \eta_1 \left(\frac{d^2 u_1}{dy^2} \right)^2 + \sigma_1 B_0^2 \lambda^2 u_1^2 + \frac{\mu_1}{K_1} u_1^2 = 0. \quad (23)$$

Concentration equation⁴⁸:

$$D_{m_1} \frac{d^2 C_1}{dy^2} + \frac{D_{m_1} k_{T_1}}{T_m} \frac{d^2 T_1}{dy^2} = 0. \quad (24)$$

The flow velocity components of couple stress fluid in upper porous zone of the duct under the above assumptions are considered as $\mathbf{v}_2 = (u_2, 0, 0)$. Due to existence of continuity equation for incompressible nature of fluid in a fully developed flow regime, the x -axis component of flow velocity will become the function of y only, i.e., $u_2 = u_2(y)$ and its y -directional velocity component vanishes.

Within the framework of above criteria, the governing flow equations for radiative, magnetized, viscous and incompressible flow regime of couple stress fluid in upper porous zone of the duct will be as follows:

Conservation of linear momentum^{33,34}:

$$\frac{dp}{dx} = \mu_2 \frac{d^2 u_2}{dy^2} - \eta_2 \frac{d^4 u_2}{dy^4} - \sigma_2 B_0^2 \lambda^2 u_2 - \frac{\mu_2}{K_2} u_2. \quad (25)$$

Conservation of energy^{33,34}:

$$\left(k_2 + \frac{16\sigma^* T_0^3}{3k^*} \right) \frac{d^2 T_2}{dy^2} + \mu_2 \left(\frac{du_2}{dy} \right)^2 + \eta_2 \left(\frac{d^2 u_2}{dy^2} \right)^2 + \sigma_2 B_0^2 u_2^2 + \frac{\mu_2}{K_2} u_2^2 = 0. \quad (26)$$

Concentration equation⁴⁸:

$$D_{m_2} \frac{d^2 C_2}{dy^2} + \frac{D_{m_2} k_{T_2}}{T_m} \frac{d^2 T_2}{dy^2} = 0. \quad (27)$$

3.2. Solution of the proposed problem

In order to reduce the nonmiscible couple stress fluid flow governing equations (22)–(27) in dimensionless form, we incorporate the following dimensionless variables:

$$u_i^* = \frac{u_i}{U_0}, \quad i = 1, 2, \quad y^* = \frac{y}{h}, \quad x^* = \frac{x}{h}, \quad n_\mu = \frac{\mu_2}{\mu_1}, \quad n_k = \frac{k_2}{k_1}, \quad \text{Da}^2 = \frac{h^2}{K_1},$$

$$\begin{aligned}
 p^* &= \frac{p}{\rho_1 U_0^2}, \quad n_\sigma = \frac{\sigma_2}{\sigma_1}, \quad \theta_i = \frac{T_i^* - T_0}{\Delta T}, \quad \text{Br} = \frac{\mu_1 U_0^2}{k_1 \Delta T}, \quad \text{Ha} = B_0 h \sqrt{\frac{\sigma_1}{\mu_1}}, \\
 \text{Re} &= \frac{\rho_1 U_0 h}{\mu_1}, \quad n_K = \frac{K_2}{K_1}, \quad s_i = \frac{\mu_i h^2}{\eta_i}, \quad \text{Nr} = \frac{4\sigma^* T_0^3}{k^* k_1}, \quad \text{Sc} = \frac{\mu_1}{\rho D_{m1}}, \\
 n_D &= \frac{D_{m2}}{D_{m1}}, \quad n_i = \frac{C_i^* - C_0}{\Delta C}, \quad \Lambda = \frac{R_{g1} D_{m1} C_0}{k_1}, \quad \text{Sr} = \frac{D_{m1} k_{T1} \nabla T \rho}{T_m \mu_1 \nabla C}, \\
 n_R &= \frac{R_{g2}}{R_{g1}}, \quad \Omega = \frac{\Delta T}{T_0}, \quad \pi = \frac{\Delta C}{C_0},
 \end{aligned}$$

where U_0 indicates the characteristics velocity of the fluid. The symbols Re, Sc, Da, Sr, Ha, Br, Nr, s_i and Λ depict the Reynolds number, Schmidt number, permeability parameter, Soret number, Hartmann number, Brinkman number, radiation parameter, couple stress parameter and diffusive constant parameter, respectively. The dimensionless ratios such as n_K , n_k , n_μ , n_σ , n_D and n_R denote the permeability ratio, thermal conductivity ratio, viscosity ratio, electrical conductivity ratio, mass diffusivity ratio and ideal gas constant ratio, respectively. The term C_0 denotes the reference concentration of the fluid. The terms Ω and π denote the dimensionless temperature and concentration ratio, respectively. The term ΔT indicates the characteristics temperature which takes the form $\Delta T = T_1^* - T_2^*$, in which $T_1^* > T_2^*$.

By incorporating these nondimensional variables into Eqs. (22)–(27) and removing the notations of *, we have Region-1 ($-h \leq y \leq 0$):

Conservation of linear momentum^{33,34}:

$$\frac{d^4 u_1}{dy^4} - s_1 \frac{d^2 u_1}{dy^2} + (\text{Da}^2 + \lambda^2 \text{Ha}^2) s_1 u_1 + \text{Re} s_1 \frac{dp}{dx} = 0. \quad (28)$$

Energy equation^{33,34}:

$$\frac{d^2 \theta_1}{dy^2} + \frac{3\text{Br}}{(3 + 4\text{Nr})} \left[\left(\frac{du_1}{dy} \right)^2 + \frac{1}{s_1} \left(\frac{d^2 u_1}{dy^2} \right)^2 + (\text{Ha}^2 \lambda^2 + \text{Da}^2) u_1^2 \right] = 0. \quad (29)$$

Concentration equation⁴⁸:

$$\frac{1}{\text{Sc}} \frac{d^2 n_1}{dy^2} + \text{Sr} \frac{d^2 \theta_1}{dy^2} = 0. \quad (30)$$

Region-2 ($0 \leq y \leq h$):

Conservation of linear momentum^{33,34}:

$$\frac{d^4 u_2}{dy^4} - s_2 \frac{d^2 u_2}{dy^2} + \left(\frac{\text{Ha}^2 \lambda^2 n_\sigma}{n_\mu} + \frac{\text{Da}^2}{n_K} \right) s_2 u_2 + \frac{\text{Res}_2 P}{n_\mu} = 0. \quad (31)$$

Energy equation^{33,34}:

$$\frac{d^2 \theta_2}{dy^2} + \frac{3\text{Br} n_\mu}{(3n_k + 4\text{Nr})} \left[\left(\frac{du_2}{dy} \right)^2 + \frac{1}{s_2} \left(\frac{d^2 u_2}{dy^2} \right)^2 + \left(\frac{\text{Ha}^2 \lambda^2 n_\sigma}{n_\mu} + \frac{\text{Da}^2}{n_K} \right) u_2^2 \right] = 0. \quad (32)$$

Concentration equation⁴⁸:

$$\frac{1}{Sc} \frac{d^2 n_2}{dy^2} + Sr \frac{d^2 \theta_2}{dy^2} = 0. \quad (33)$$

On solving the governing equations (28)–(33) by using reliable technique, authors obtained the closed form expressions for temperature distribution and flow behavior of immiscible nature of couple stress fluid in bottom and upper porous zone of the duct, which are given in Appendix A.

3.3. Boundary conditions

The classical no-slip boundary conditions at the lower ($y = -1$) and upper ($y = 1$) porous wall of the conduit are taken as³³

$$u_1(-1) = 0, \quad u_2(1) = 0. \quad (34)$$

The boundary condition on the couple stresses which vanishes at the lower and upper porous wall of the duct¹⁶ is taken as

$$\frac{d^2 u_1}{dy^2} = 0 \quad \text{at } y = -1, \quad \frac{d^2 u_2}{dy^2} = 0 \quad \text{at } y = 1. \quad (35)$$

At the interfacial region $y = 0$, we consider that the couple stress, flow velocity component, vorticity component and shear stress components are continuous,³³ i.e.,

$$u_1(0) = u_2(0), \quad (36)$$

$$\frac{du_1(0)}{dy} = \frac{du_2(0)}{dy}, \quad (37)$$

$$\left(s_1 \frac{du_1}{dy} - \frac{d^3 u_1}{dy^3} \right) = n_\eta \left(s_2 \frac{du_2}{dy} - \frac{d^3 u_2}{dy^3} \right), \quad (38)$$

$$\left(\frac{d^2 u_1}{dy^2} \right) = n_\eta \left(\frac{d^2 u_2}{dy^2} \right). \quad (39)$$

The thermal boundary conditions at the bottom, top and central zone of the porous duct are described as

- (1) The thermal distribution at the bottom and top porous wall of the channel is given as³³

$$\theta_1(-1) = 0, \quad \theta_2(1) = 1. \quad (40)$$

- (2) The continuity of thermal distribution and heat flux at the interfacial region of the fluid is addressed as³³

$$\theta_1(0) = \theta_2(0), \quad \frac{d\theta_1}{dy} = n_k \frac{d\theta_2}{dy} \quad \text{at } y = 0. \quad (41)$$

The concentration profile at the bottom and upper isothermal plates of the porous duct is given by⁵²

$$n_1 = 0 \quad \text{at } y = -1, \tag{42}$$

$$n_2 = 1 \quad \text{at } y = 1. \tag{43}$$

The concentration profile of immiscible fluids is continuous at the interfacial region,⁵² i.e.,

$$n_1(y) = n_2(y) \quad \text{at } y = 0, \tag{44}$$

$$\frac{dn_1}{dy} = n_D \frac{dn_2}{dy} \quad \text{at } y = 0. \tag{45}$$

The above boundary conditions have been used to obtain the arbitrary constants appearing in the solution of governing Eqs. (28)–(33) which is given in Appendix A with the help of Mathematica Software 10.3.

4. Production of Entropy and Bejan Number Distribution for Immiscible Nature of Couple Stress Fluid in a Porous Saturated Domain

4.1. Generation of entropy inside a porous saturated pipe

Entropy production is a crucial thermal parameter and it determines the reason of the loss of useful energy in any engineering and thermal process which includes the heat exchange, mass exchange and fluid flow process. The convection heat exchange and fluid transportation through a porous material are essentially irreversible in environment. Production of entropy in a thermal and fluid flow process arises because of thermal energy exchange and transfer of momentum between the impermeable walls and within the fluid medium of the conduit. In the present model, the entropy produces because of the thermal exchange irreversibility, magnetic effect irreversibility, radiative thermal exchange irreversibility, irreversibility due to porous media, fluid frictional irreversibility and irreversibility due to mass transfer.

The volumetric entropy production rate due to couple stress fluid flow in a lower porous region of the duct under the impact of radiative heat exchange and mass exchange is given by^{25,53}

$$\begin{aligned} (S_1)_G = & \frac{k_1}{T_0^2} \left[1 + \frac{16\sigma^* T_0^3}{3k^* k_1} \right] \left(\frac{\partial T_1}{\partial y} \right)^2 + \frac{\mu_1}{T_0} \left(\frac{\partial u_1}{\partial y} \right)^2 + \frac{\eta_1}{T_0} \left(\frac{\partial^2 u_1}{\partial y^2} \right)^2 \\ & + \frac{\sigma_1 B_0^2 \lambda^2 u_1^2}{T_0} + \frac{\mu_1}{K_1 T_0} u_1^2 + \frac{R_{g1} D_{m1}}{C_0} \left(\frac{\partial C_1}{\partial y} \right)^2 + \frac{R_{g1} D_{m1}}{T_0} \\ & \times \left(\frac{\partial C_1}{\partial y} \frac{\partial T_1}{\partial y} \right). \tag{46} \end{aligned}$$

The volumetric entropy production rate due to flow regime of couple stress fluid within the upper porous region of the duct under the impact of radiative heat

exchange and mass exchange is given by^{25,53}

$$(S_2)_G = \frac{k_2}{T_0^2} \left[1 + \frac{16\sigma^* T_0^3}{3k^* k_2} \right] \left(\frac{\partial T_2}{\partial y} \right)^2 + \frac{\mu_2}{T_0} \left(\frac{\partial u_2}{\partial y} \right)^2 + \frac{\eta_2}{T_0} \left(\frac{\partial^2 u_2}{\partial y^2} \right)^2 + \frac{\sigma_2 B_0^2 \lambda^2 u_2^2}{T_0} + \frac{\mu_2}{K_2 T_0} u_2^2 + \frac{R_{g_2} D_{m_2}}{C_0} \left(\frac{\partial C_2}{\partial y} \right)^2 + \frac{R_{g_2} D_{m_2}}{T_0} \left(\frac{\partial C_2}{\partial y} \frac{\partial T_2}{\partial y} \right) \quad (47)$$

Note that first, fourth and fifth terms in Eqs. (46) and (47) highlight the generation of entropy in their respective region of the duct because of radiative thermal exchange, existence of magnetic field and presence of porous media, however, the second and third term indicates entropy production distribution in respective region due to fluid friction. The sixth and seventh terms denote the generation of entropy in their respective region of the duct because of mass diffusion and coupling between heat and mass diffusion, respectively.

Based on the concept of minimization of entropy, the characteristics rate of entropy production is given by^{25,53}

$$S_{G,C} = \left[\frac{k_1 (\Delta T)^2}{h^2 T_0^2} \right]. \quad (48)$$

The dimensionless form of entropy production number for incompressible, radiative, magnetized and immiscible nature of couple stress fluid in the lower and upper porous region, respectively, of the duct is expressed as

$$N_{s_1} = \left(1 + \frac{4}{3} Nr \right) \left(\frac{d\theta_1}{dy} \right)^2 + \frac{Br}{\Omega} \left[\left(\frac{du_1}{dy} \right)^2 + \frac{1}{s_1} \left(\frac{d^2 u_1}{dy^2} \right)^2 + (Ha^2 \lambda^2 + Da^2) u_1^2 \right] + \Lambda \left(\frac{\pi}{\Omega} \right) \left[\left(\frac{\pi}{\Omega} \right) \left(\frac{dn_1}{dy} \right)^2 + \left(\frac{dn_1}{dy} \frac{d\theta_1}{dy} \right) \right], \quad (49)$$

$$N_{s_2} = \left(1 + \frac{4Nr}{3n_k} \right) \left(\frac{d\theta_2}{dy} \right)^2 + \frac{Br}{\Omega} \frac{n_\mu}{n_k} \left[\left(\frac{du_2}{dy} \right)^2 + \frac{1}{s_2} \left(\frac{d^2 u_2}{dy^2} \right)^2 + \left(\frac{Ha^2 \lambda^2 n_\sigma}{n_\mu} + \frac{Da^2}{n_k} \right) u_2^2 \right] + \Lambda \frac{n_D n_R}{n_k} \left(\frac{\pi}{\Omega} \right) \left[\left(\frac{\pi}{\Omega} \right) \left(\frac{dn_2}{dy} \right)^2 + \left(\frac{dn_2}{dy} \frac{d\theta_2}{dy} \right) \right]. \quad (50)$$

Equations (49) and (50) can be classified by the following relation:

$$N_{s_i} = N_{y_i} + N_{f_i}. \quad (51)$$

Here, N_{y_i} highlights the generation of entropy due to radiative thermal exchange and N_{f_i} denotes the entropy generation due to mass transfer, porous media, magnetic field and viscous dissipation.

4.2. Bejan number distribution

The term irreversibility distribution ratio (p_i) is defined as the division of entropy production (N_{f_i}) due to fluid friction, presence of porous media, applied magnetic

field and mass transfer to the production of entropy (Ny_i) due to radiative thermal exchange, i.e.,

$$p_i = \frac{Nf_i}{Ny_i}, \quad i = 1, 2. \tag{52}$$

If the irreversibility distribution arises due to fluid friction, presence of porous media, applied magnetic field and mass transfer then $p_i > 1$, but if it arises due to thermal exchange, then $0 < p_i < 1$. It is noticed that if the irreversibility arises due to combined effect of fluid friction, presence of porous media, applied magnetic field, mass transfer and thermal exchange, then $p_i = 1$.⁵³

A crucial thermodynamic parameter which is used in advanced thermodynamic analysis is known as Bejan number.⁵⁴ It is defined as the fraction of entropy production originated by radiative heat exchange to the total generation of entropy within the porous conduit.⁵⁵

$$Be_i = \frac{Ny_i}{Ns_i} = \frac{Ny_i}{Ny_i + Nf_i} = \frac{1}{1 + p_i}, \quad i = 1, 2. \tag{53}$$

On the basis of physical significance, the classification of Bejan number distribution is described in three different categories. From Eq. (53), $Be = 0$ illustrates that irreversibility distribution due to heat exchange is zero, $Be = 1$ depicts that the irreversibility distribution by viscous dissipation, applied magnetic field, presence of porous media and mass transfer is negligible. $Be = 0.5$ describes that irreversibility distribution due to radiative heat exchange and other parameters such as magnetic field, mass transfer, porous media and viscous dissipation are same.

The Bejan number distribution in lower and upper porous zone, respectively, of the duct for radiative, magnetized couple stress fluid which flows in respective region is given as

$$Be_1 = \frac{\left(1 + \frac{4}{3}Nr\right) \left(\frac{d\theta_1}{dy}\right)^2}{Ns_1}, \tag{54}$$

$$Be_2 = \frac{\left(1 + \frac{4Nr}{3n_k}\right) \left(\frac{d\theta_2}{dy}\right)^2}{Ns_2}, \tag{55}$$

where Ns_1 and Ns_2 are given in Eqs. (49) and (50), respectively.

5. Analysis of Result

The examination of the entropy production in different geometrical configurations under varying conditions has dynamic applications in rotating mechanical devices, industrial equipment optimization and improving the performance of many engineering technologies. Many creative studies have been published in recent years because second law analysis is useful for getting the best design for the system. Additionally, the analysis of nonmiscible fluid flow and heat exchange has

significance in the movement of crude oil and transportation procedures. In the present nonmiscible flow model, we considered the flow of nonmiscible couple stress fluid in a horizontal porous conduit under the impact of oriented magnetic field and radiative thermal exchange. In this flow problem, we examine the entropy generation distribution, flow characteristics, Bejan number and heat transfer of nonmiscible couple stress fluid within a horizontal porous duct. The presence of porous material in the flowing fluid increases the amount of drag, friction and flow resistance between the fluid flow and porous solid surfaces. In order to obtain exact solutions for thermal behavior, flow velocity, entropy production characteristics and Bejan number distribution, we employed the reliable technique in this problem. Here, we mainly focus to discuss on the behaviors of pertinent thermo-physical parameters such as Hartmann number, permeability parameter and couple stress parameter, Schmidt number and Soret number on entropy generation number, flow velocity, Bejan number and thermal characteristics of nonmiscible type of couple stress fluid within a horizontal porous pipe. In order to validate the numerical values of various flow parameters, we take some references of earlier published papers.^{28,29,31-35} From the previous published literature, it is noticed that the dimensionless pressure gradient takes the estimated values between $(-\infty, 0)$,³⁴ the Hartmann number assumes the values between $[0, \infty)$,³⁴ radiation parameter takes the values between $(0, \infty)$,^{33,35} permeability parameter lies in the interval $[0, \infty)$ ³⁹ and the couple stress parameter lies in $(0, \infty)$.³⁴

5.1. Couple stress parameter impact on flow properties

The impact of couple stress parameter over the physical variables such as flow distribution, entropy generation number, thermal profile and Bejan number distribution has been discussed in this section. Figures 2 and 3 promulgate the couple stress parameter effect on flow distribution and temperature profile of immiscible

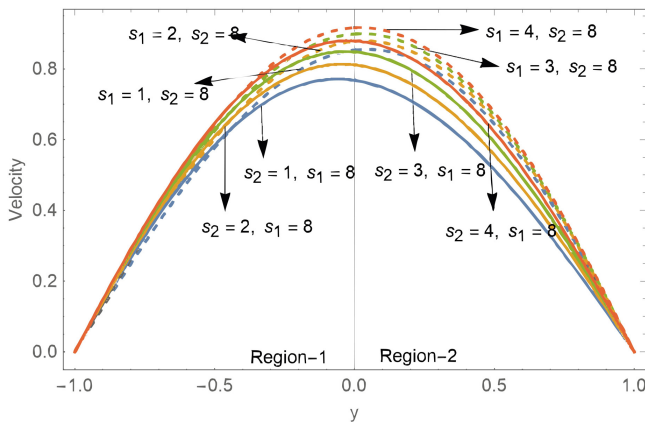


Fig. 2. (Color online) Velocity profile with couple stress parameter.

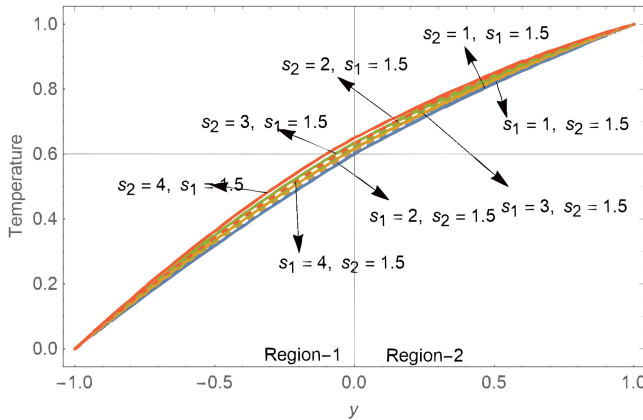


Fig. 3. (Color online) Temperature profile with couple stress parameter.

couple stress fluid in a rectangular porous pipe, respectively, when $P = -1.5$, $Da = 0.1$, $Ha = 0.5$, $\lambda = 0.5$, $Nr = 1$, $s_1 = 1.5$, $n_K = 1.2$, $Re = 2$, $Br = 0.5$, $\Omega = 1$, $n_\mu = 0.9$, $n_k = 1.1$, $n_\sigma = 0.6$, $n_\eta = 0.7$. From Fig. 2, we concluded that ascending trend in couple stress fluid parameter accelerates the flow velocity in the porous conduit. This would be explained by the fact that the couple stresses expend some energy in rotating the fluid particles, which causes the reduction of flow velocity of immiscible couple stress fluid in the porous channel. Figure 3 depicts the variation of temperature profile of immiscible couple stress fluid with the ascending values of couple stress parameter in the porous medium. From this plot, we analyzed that the thermal characteristics of immiscible fluid get boosted by enlargement of couple stress parameter within the porous flow domain. Physically, this is accurate due to the fluid's diminishing dynamic viscosity. The results show that the fluid temperature increases in the areas close to interface of immiscible fluid, however, the fluid temperature decreases towards the heated wall of the porous channel. However, as the viscous forces of the fluid reduce along with the couple stress parameter, the degree of freedom of the immiscible fluid particles also lowers, which will ultimately lead to a reduction in the temperature distribution within the porous channel. It is also concluded that couple stress parameter s_1 of porous Region-1 shows much effect on temperature profile as comparison to the couple stress parameter s_2 of upper porous region. These findings are well in agreement with the research work published by Ref. 32.

The science behind this findings is that the reduction in couple stress parameter enhances the dynamic viscosity of immiscible type of couple stress fluid which reduces the flow velocity. This result is validated with the works published by Refs. 32, 34 and 57.

The dependency of entropy production number with the ascending values of couple stress parameter when $P = -20.0$, $Da = 0.1$, $Ha = 0.5$, $\lambda = 0.5$, $Nr = 2$, $s_2 = 8$, $n_K = 1.2$, $Re = 2$, $Br = 0.8$, $\Omega = 1$, $n_\mu = 0.9$, $n_k = 1.1$, $n_\sigma = 0.9$, $n_\eta = 1.1$ is

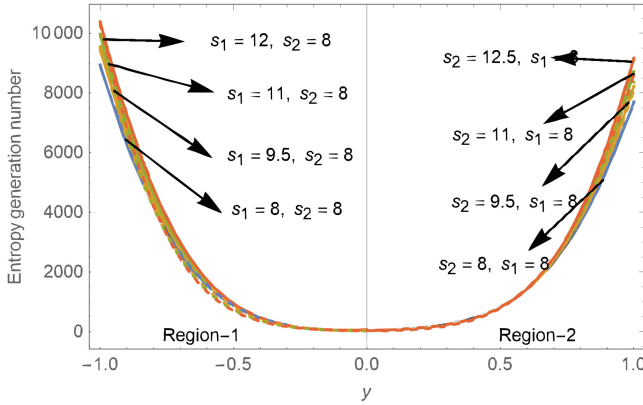


Fig. 4. (Color online) Entropy generation number with couple stress parameter.

illustrated in Fig. 4. From this plot, we examined that the ascending trend of couple stress parameter enhances the production of entropy nearby the wall of the porous conduit. From the given figure, we observe that couple stress parameter illustrates very less or negligible effect on the entropy production number at the interfacial region of the porous pipe. This is expected because, as seen in Figs. 2 and 3, the couple stress parameter raises both the temperature and flow velocity of immiscible couple stress fluids within the porous saturated channel. Additionally, Fig. 4 shows that heat transfer rises the irreversibility ratio at the channel walls because of an increase in the kinetic energy of the fluid particles, whereas viscosity predominates in the channel center. It is also examined that the entropy production number achieved its lower value at the interfacial zone of nonmiscible fluid. This result may be used in making the thermo-fluid model as energetically efficient as possible. The impact of couple stress parameter on Bejan number distribution when $P = -0.1$, $Da = 0.1$, $Ha = 0.1$, $\lambda = 0.1$, $Nr = 1$, $s_2 = 5$, $n_K = 0.9$, $Re = 2.5$, $Br = 5$, $\Omega = 1$, $n_\mu = 0.9$, $n_k = 0.9$, $n_\sigma = 0.9$, $n_\eta = 0.9$ is illustrated in Fig. 5. It is concluded that the ascending values of couple stress parameter enhance the Bejan number distribution at the interfacial region of immiscible fluid. The reason behind the above fact is that as the couple stress parameter grows, the fluid's flow velocity and temperature rise, which improves viscous heating and thermal dissipation and hence Bejan number profile enhances at the interfacial region of immiscible fluid. A similar nature of plot is reported in the works of Refs. 32 and 34 which validate our results.

5.2. Impact of Hartmann number Ha

Here, we discuss the impact of Hartmann number on various flow properties such as entropy production characteristics, Bejan number distribution, thermal profile and flow regime of immiscible type of couple stress fluid. Figures 6 and 7 are aimed to elucidate the impact of Hartmann number profile on flow behavior and temperature of immiscible type of couple stress fluid within the porous conduit when $P = -1.5$,

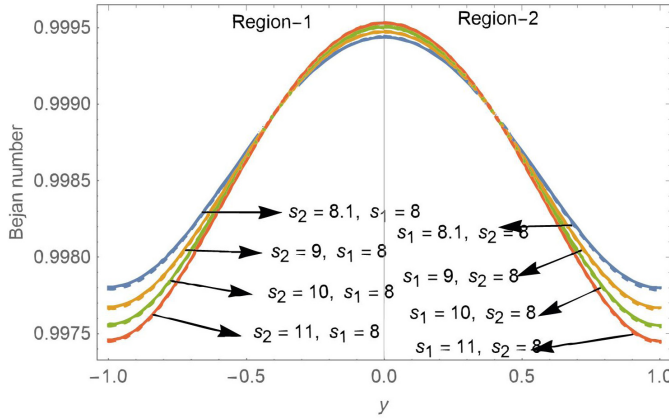


Fig. 5. (Color online) Bejan number with couple stress parameter.

Da = 0.1, Nr = 2, $\lambda = 0.5$, $s_2 = 8$, $n_K = 1.2$, $s_1 = 18$, Re = 2, Br = 0.7, $\Omega = 1$, $n_\mu = 0.9$, $n_k = 1.1$, $n_\sigma = 0.9$, $n_\eta = 1.1$. These figures conclude that the magnetic field shows the same kind of effect on the flow behavior and temperature profile of immiscible couple stress fluid as couple stress parameter does. From Fig. 6, we examined that the couple stress fluid velocity diminishes with the ascending values of Hartmann number. In other words, we can say that the couple stress fluid velocity can be suppressed by boosting the applied magnetic field strength. This is due to the fact that the applied magnetic field which is perpendicular to the flow direction tends to control the motion of the fluids in the channel by creating a retarding force called the Lorentzian drag force that acts in the opposite direction of the flow. This phenomenon takes place due to resistive impact of Lorentzian drag force which arises because of applied magnetic field in the flow domain.

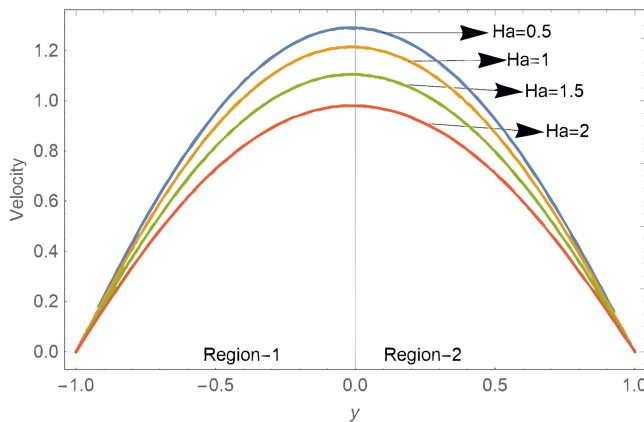


Fig. 6. (Color online) Velocity profile with Ha.

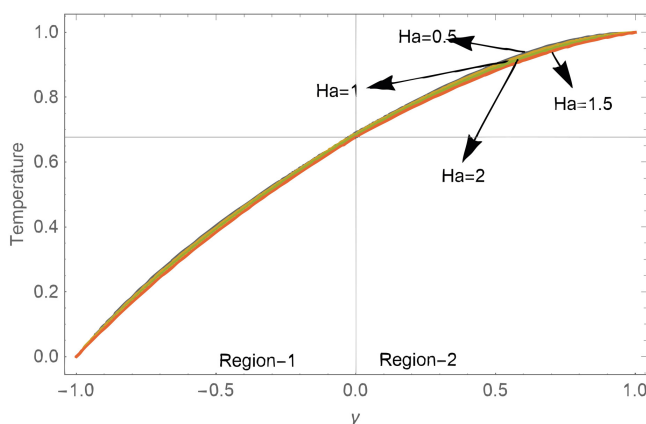


Fig. 7. (Color online) Temperature distribution with Ha.

It is noticeable because of its enormous applications in the metal industries where the hot fluid flow controls during the metal processing mechanism. In Fig. 7, dependency of thermal characteristics with various favorable values of Ha is portrayed. This graph illustrates that the temperature profile diminishes on increasing values of magnetic field strength. Figure 8 describes the impact of Ha on entropy generation characteristics of immiscible couple stress fluid inside the porous conduit when $P = -1.5$, $Da = 0.1$, $s_1 = 8$, $\lambda = 0.5$, $n_\eta = 1.1$, $Re = 35$, $s_2 = 8$, $n_k = 1.1$, $n_\mu = 1.1$, $n_\sigma = 1.1$, $n_K = 1.1$, $Nr = 1$, $Br = 0.5$, $n_D = 1.1$, $Sc = 5$, $Sr = 0.6$, $\Lambda = 0.1$, $\pi = 0.3$, $\Omega = 0.1$, $n_R = 1.1$. This plot elucidates that the production of entropy decreases with the enlargement of magnetic field intensity parameter Ha nearby the plates of the porous duct. Hence, Ha can be utilized to control the generation of entropy in the flow medium. From this plot, it is examined that the entropy production number achieved extremum values in the lower porous region as compared to upper porous region of the duct. The rise of entropy generations caused by heat conduction and

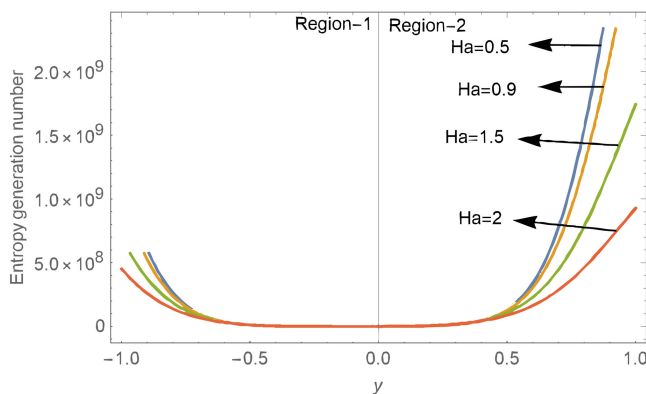


Fig. 8. (Color online) Entropy generation number with Ha.

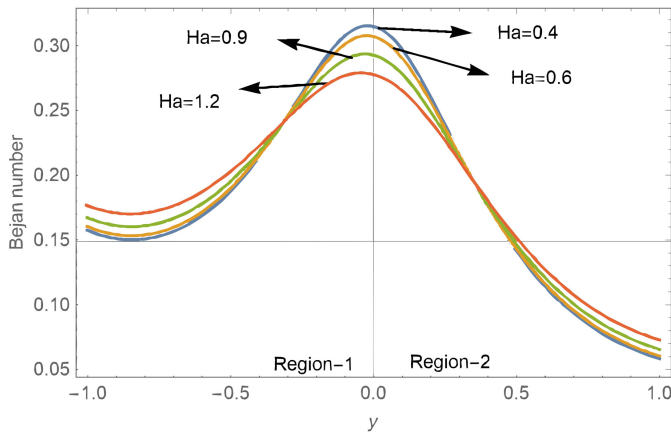


Fig. 9. (Color online) Bejan number with Ha.

conducting fluid friction in immiscible couple stress fluids can be significantly lessen or stopped by increasing the Hartmann number. It can be analyzed from Fig. 9 that the Bejan number distribution enhances on ascending values of Ha when $P = -0.1$, $Da = 0.1$, $s_1 = 8$, $\lambda = 0.5$, $n_\eta = 1.1$, $Re = 35$, $s_2 = 8$, $n_k = 1.1$, $n_\mu = 1.1$, $n_\sigma = 1.1$, $n_K = 1.1$, $Nr = 1$, $Br = 0.1$, $n_D = 1.1$, $Sc = 2$, $Sr = 2$, $\Lambda = 0.1$, $\pi = 0.1$, $\Omega = 0.1$, $n_R = 1.1$. The nature of plots of flow velocity, entropy production characteristics, thermal profile and Bejan number distribution with Ha shows excellent agreement with the work of Refs. 33 and 34.

5.3. Influence of permeability parameter Da on flow properties

In this section, the permeability parameter effects on thermal characteristics, entropy production number, velocity distribution and Bejan number distribution for immiscible couple stress fluid in both the porous zone of the duct are discussed. Figures 10 and 11 represent the impact of permeability parameter on the flow characteristics and temperature of nonmiscible type of couple stress fluids in the porous domain when $P = -1.5$, $Ha = 0.5$, $Nr = 2$, $\lambda = 0.5$, $s_2 = 8$, $n_K = 1.2$, $s_1 = 18$, $Re = 2$, $Br = 0.7$, $\Omega = 1$, $n_\mu = 0.9$, $n_k = 1.1$, $n_\sigma = 0.9$, $n_\eta = 1.1$. We observed from Fig. 10 that an ascending trend in permeability parameter leads to reduction in the movement of the fluid within the porous domain. This is so because the permeable nature of porous material reduces on increasing the permeability parameter and it develops resistance to the flow field and hence the flow distribution of immiscible type of fluid decreases. This result is authenticated by the investigation of Refs. 39 and 56.

It is examined from Fig. 11 that the permeability parameter reduces the thermal profile of couple stress fluid in both the regions of the flow conduit. This result shows that less permeable medium reduces heat transfer within the porous medium.

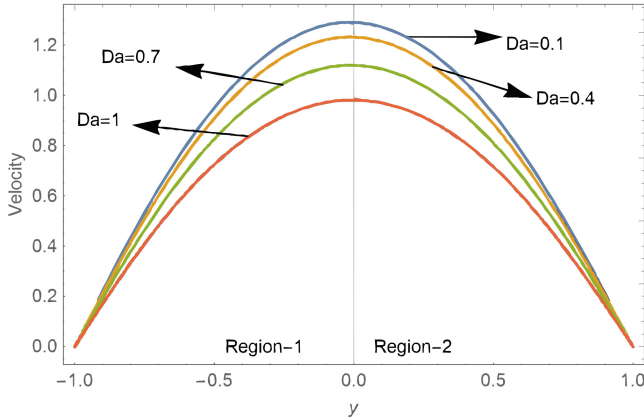


Fig. 10. (Color online) Velocity profile with Da.

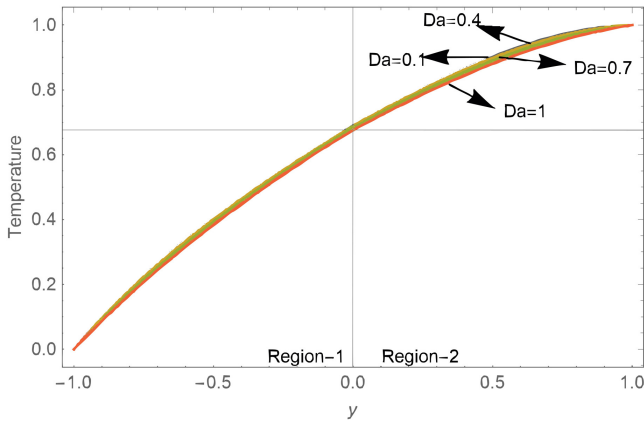


Fig. 11. (Color online) Temperature profile with Da.

This result is approved with the work of Ref. 58. This figure illustrates that the temperature profile attains extremum value in upper porous region of the duct.

Figure 12 has been plotted to analyze the production of entropy against the permeability parameter when $P = -1.5$, $s_1 = 8$, $H = 0.5$, $\lambda = 0.5$, $n_\eta = 1.1$, $Re = 35$, $s_2 = 8$, $n_k = 1.1$, $n_\mu = 1.1$, $n_\sigma = 1.1$, $n_K = 1.1$, $Nr = 1$, $Br = 0.5$, $n_D = 1.1$, $Sc = 5$, $Sr = 0.6$, $\Lambda = 0.1$, $\pi = 0.3$, $\Omega = 0.1$, $n_R = 1.1$ and concluded that entropy generation reduces as the permeability parameter increases in both the region of the porous conduit. Entropy production in porous media is primarily dominated by the drag and friction forces between the flow and the porous solids. Figure 13 is presented to discuss the impact of permeability parameter on the Bejan number profile of immiscible couple stress fluid in the porous medium when $P = -0.1$, $Ha = 0.5$, $s_1 = 8$, $\lambda = 0.5$, $n_\eta = 1.1$, $Re = 35$, $s_2 = 8$, $n_k = 1.1$, $n_\mu = 1.1$, $n_\sigma = 1.1$, $n_K = 1.1$,

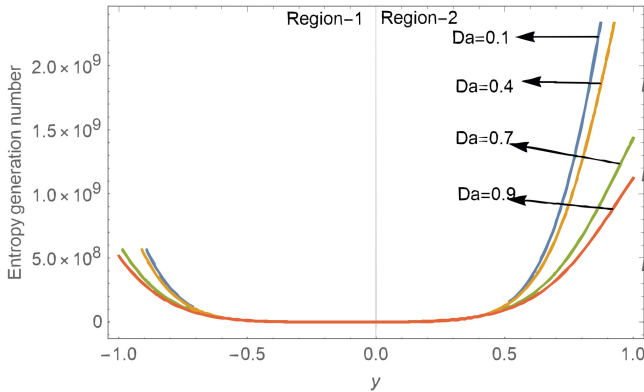


Fig. 12. (Color online) Entropy generation number with Da.

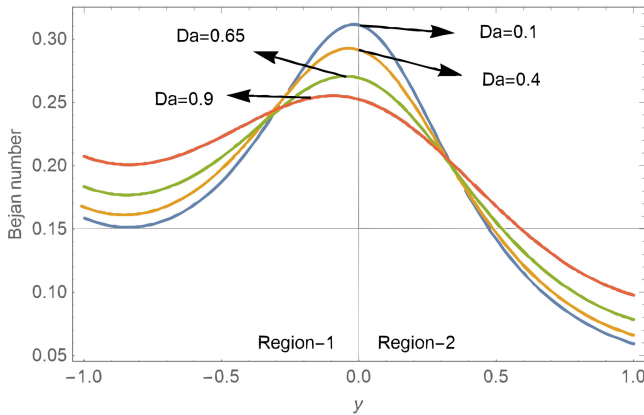


Fig. 13. (Color online) Bejan number with Da.

$Nr = 1$, $Br = 0.1$, $n_D = 1.1$, $Sc = 2$, $Sr = 2$, $\Lambda = 0.1$, $\pi = 0.1$, $\Omega = 0.1$, $n_R = 1.1$. From this plot, we concluded that Bejan number diminishes with the ascending values of permeability parameter nearby the interfacial region of the conduit, however Bejan number gets enhanced on increasing the permeability parameter in the other region of the porous conduit. This result is validated with the work done by Refs. 33 and 34.

5.4. Impact of Schmidt number Sc

In this section, the influence of Schmidt number on entropy generation number, concentration distribution and Bejan number profile of immiscible type of couple stress fluid in a porous saturated duct is discussed. The Schmidt number describes the relative ease of mass exchange and molecular momentum and is very crucial in computations of binary mass transfer in various multiphase flows. Schmidt numbers

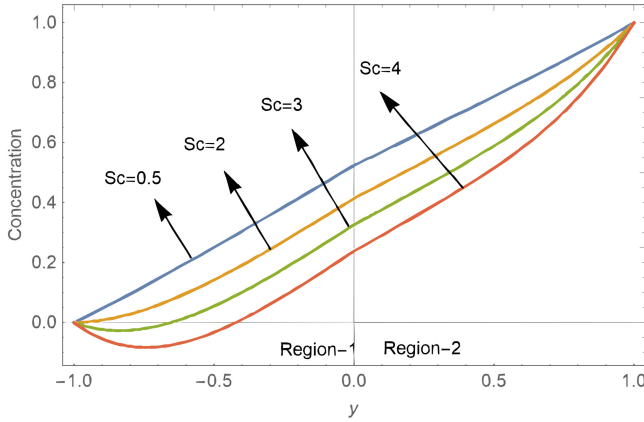


Fig. 14. (Color online) Concentration profile with Schmidt number Sc .

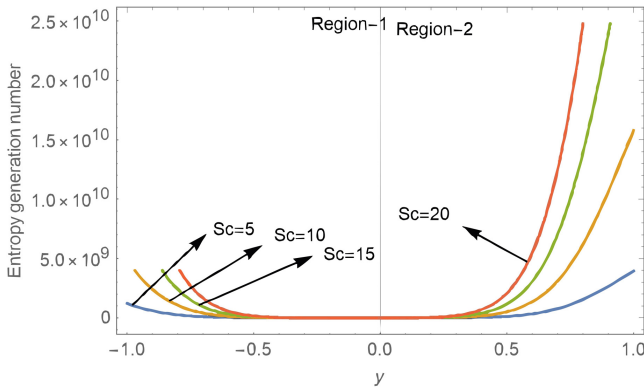


Fig. 15. (Color online) Entropy generation number with Schmidt number Sc .

for the most interesting chemical species that diffuse in air range from 0.1 to 10. Figures 14 and 15 illustrate the impact of Schmidt number on concentration profile and entropy production number of immiscible type of couple stress fluid in a porous saturated duct when $P = -1.5$, $Da = 0.1$, $Ha = 0.5$, $\lambda = 0.5$, $Nr = 1$, $s_2 = 8$, $n_K = 1.2$, $s_1 = 8$, $Re = 2$, $Br = 0.8$, $\Omega = 1$, $n_\mu = 0.9$, $n_k = 1.1$, $n_\sigma = 0.6$, $n_\eta = 0.7$, $\Omega = 0.3$, $\Lambda = 0.3$, $\pi = 0.3$, $Sr = 0.6$, $n_D = 1.2$, $n_R = 2$. From Fig. 14, we observed that the concentration profile of immiscible fluid decreases with the enhancing values of Schmidt number Sc . This demonstrates that heavier diffusing molecules have a stronger retarding influence on the flow field's concentration distribution. The physics behind this is that the extremum values of Schmidt number lead to decrease in the mass diffusivity, which diminishes the concentration distribution of immiscible type of couple stress in a porous saturated duct. According to Fig. 14, a rise in the Schmidt number signifies a decrease in the solute diffusivity, which results in a

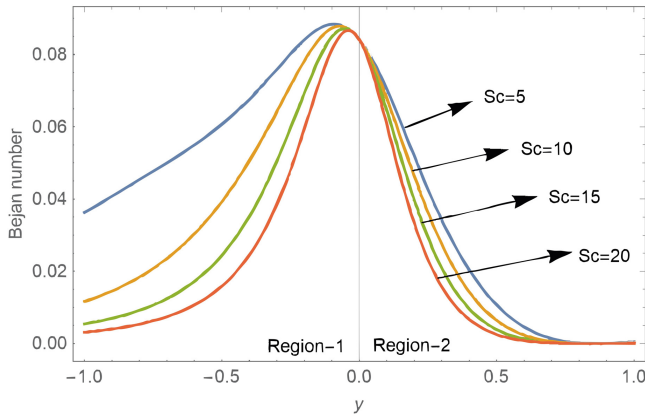


Fig. 16. (Color online) Bejan number with Schmidt number Sc .

shallower penetration of the solute effect. Therefore, as Sc levels rise, concentration falls. The concentration profile attains extremum values in upper porous channel as compared to lower porous channel. This finding correlates fairly well with Refs. 59 and 60. The entropy generation increases significantly towards the wall of the duct while it is slightly minimum at the interfacial zone of the duct (Fig. 15). It is noticeable that the entropy production attains higher values in upper porous region of the channel. Our results with entropy production number versus Schmidt number are well verified with Ref. 61. The dependency of Bejan number with various favorable values of Schmidt number when $P = -0.1$, $Da = 0.1$, $Ha = 0.5$, $\lambda = 0.5$, $Nr = 1$, $s_2 = 8$, $n_K = 1.1$, $s_1 = 8$, $Re = 35$, $Br = 0.8$, $\Omega = 1$, $n_\mu = 1.1$, $n_k = 1.1$, $n_\sigma = 1.1$, $n_\eta = 1.1$, $\Omega = 0.1$, $\Lambda = 0.1$, $\pi = 0.1$, $Sr = 5$, $n_D = 1.1$, $n_R = 1.1$ is displayed in Fig. 16. From this plot, we observed that the increasing values of Schmidt

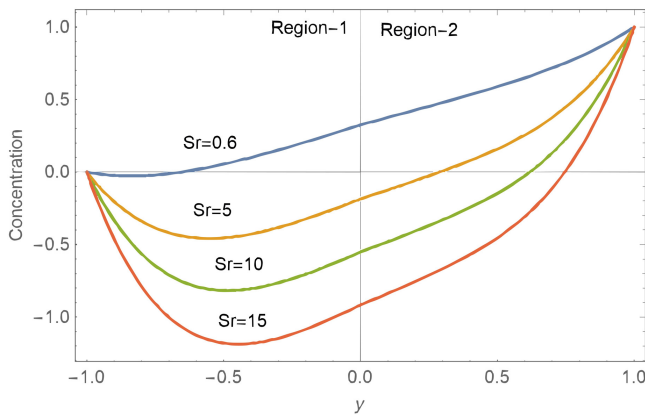


Fig. 17. (Color online) Concentration profile with Soret number, when $P = -1.5$, $Da = 0.1$, $Ha = 0.5$, $\lambda = 0.5$, $Nr = 1$, $s_2 = 8$, $n_K = 1.2$, $s_1 = 8$, $Re = 2$, $Br = 0.8$, $\Omega = 1$, $n_\mu = 0.9$, $n_k = 1.1$, $n_\sigma = 0.6$, $n_\eta = 0.7$, $\Omega = 0.3$, $\Lambda = 0.3$, $\pi = 0.3$, $Sr = 0.6$, $n_D = 1.2$, $n_R = 2$.

number enhance the Bejan number profile of immiscible type of couple stress fluid in a rectangular porous pipe.

5.5. Impact of Soret number Sr

The impact of Soret number Sr on various flow properties such as entropy generation number, concentration and Bejan number profile is displayed in Figs. 17–19. The concentration field of immiscible nature of couple stress fluid for various favorable values of Soret number Sr is illustrated in Fig. 17. It is observed that the concentration profile of immiscible fluid diminishes with the ascending trend of Soret number Sr . From this figure, it reveals that the concentration profile of couple stress

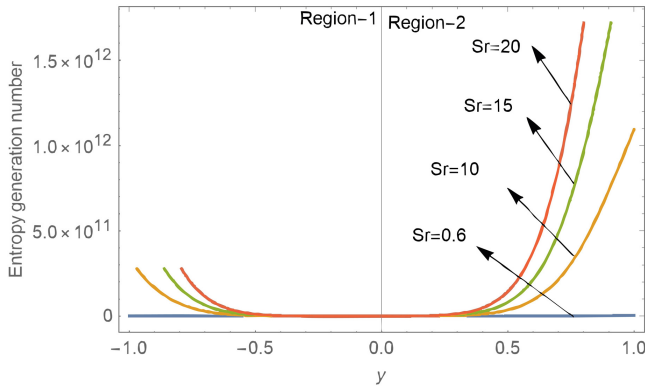


Fig. 18. (Color online) Entropy generation number with Soret number when $P = -1.5$, $Da = 0.1$, $Ha = 0.5$, $\lambda = 0.5$, $Nr = 1$, $s_2 = 8$, $n_K = 1.2$, $s_1 = 8$, $Re = 35$, $Br = 0.5$, $\Omega = 0.1$, $n_\mu = 1.1$, $n_k = 1.1$, $n_\sigma = 1.1$, $n_\eta = 1.1$, $\Omega = 0.1$, $\Lambda = 0.1$, $\pi = 0.3$, $Sr = 0.6$, $n_D = 1.1$, $n_R = 1.1$.

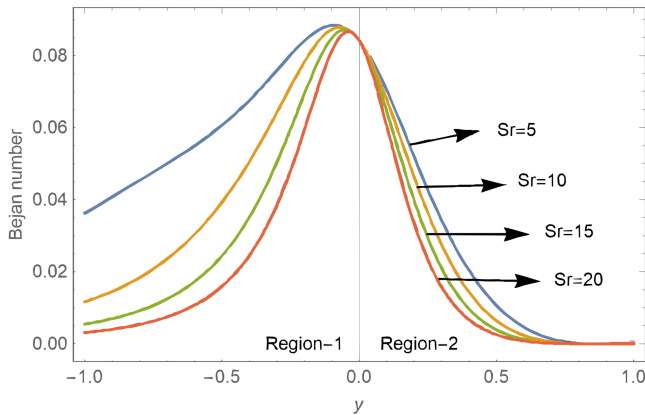


Fig. 19. (Color online) Bejan number with Soret number when $P = -0.1$, $Da = 0.1$, $Ha = 0.5$, $\lambda = 0.5$, $Nr = 1$, $s_2 = 8$, $n_K = 1.1$, $s_1 = 8$, $Re = 35$, $Br = 0.8$, $\Omega = 1$, $n_\mu = 1.1$, $n_k = 1.1$, $n_\sigma = 1.1$, $n_\eta = 1.1$, $\Omega = 0.1$, $\Lambda = 0.1$, $\pi = 0.1$, $Sc = 5$, $n_D = 1.1$, $n_R = 1.1$.

fluid with the increasing values of Soret number Sr in upper porous region (Region-2) is higher as compared to lower porous region of the channel. The impact of Soret number on entropy production of immiscible type of couple stress fluid in a porous saturated duct is depicted in Fig. 18. Figure 18 illustrates that ascending values of Sr enhance the production of entropy for immiscible nature of couple stress fluid in a porous saturated channel. Ascending values of Sr enhance the entropy production at the upper wall of the conduit while small increment is noticed on the lower wall of the duct. The variations in Bejan number profile of immiscible couple stress fluid due to the increase of Soret number are displayed in Fig. 19. It is clearly examined that the Bejan number diminishes with the ascending values of Sr .

6. Particular Case

6.1. When two immiscible fluids are Newtonian and Newtonian

When $\eta_1 \rightarrow 0$ and $\eta_2 \rightarrow 0$, i.e., $s_1 \rightarrow \infty$ and $s_2 \rightarrow \infty$ in Eqs. (47)–(52), the aforementioned model will reduce to a model of two immiscible (Newtonian–Newtonian) fluids flow through porous channel under the impact of thermal radiation and magnetic field. The comparison of flow velocity and concentration field for both the cases of immiscible fluids (couple stress–couple stress fluids and Newtonian–Newtonian fluids) is shown in Figs. 20 and 21. In these figures, the dotted lines show the variation in flow velocity and concentration field for immiscible Newtonian–Newtonian fluid model whereas the solid lines depicts the variation in flow velocity and concentration field for couple stress–couple stress fluid model. From these figures, it can be concluded that the flow velocity and concentration field for the two-fluid system (Newtonian–Newtonian) is greater than the flow velocity and concentration field of immiscible couple stress–couple stress fluid. Our results correlate favorably well with the work.⁶²

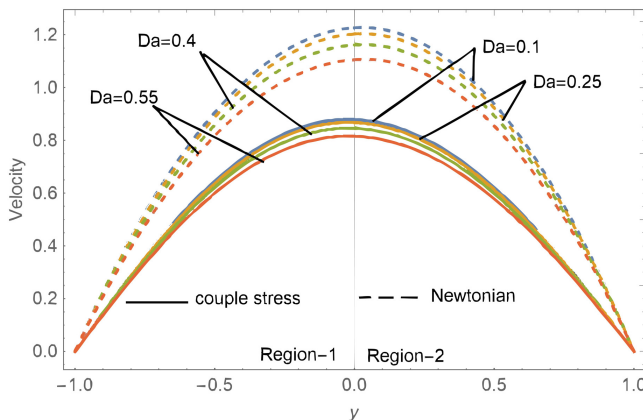


Fig. 20. (Color online) Velocity profile with Da when $P = -0.1$, $Re = 2$, $Ha = 0.5$, $\lambda = 0.5$, $n_K = 1.2$, $n_k = 1.1$, $n_\sigma = 0.9$, $n_\mu = 0.9$.

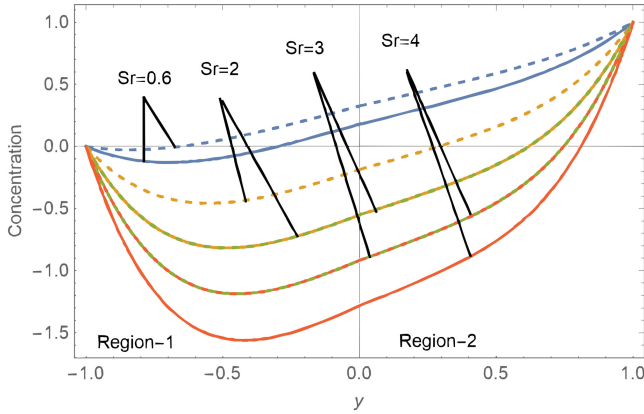


Fig. 21. (Color online) Concentration profile with Sr when $P = -0.9$, $Da = 0.1$, $Re = 2$, $Ha = 0.5$, $\lambda = 0.5$, $n_K = 1.2$, $n_k = 1.1$, $n_\sigma = 0.9$, $n_\mu = 0.6$, $Br = 0.5$, $Nr = 1$, $n_D = 1.1$, $Sc = 5$.

7. Conclusion

In the present flow problem, convective heat transfer, flow velocity, Bejan number and entropy production number of two nonmiscible couple stress fluid within a porous medium had been analyzed. To the best of authors' knowledge, the production of entropy and Bejan number due to concentration distribution of nonmiscible couple stress fluid in a porous saturated medium is not discussed yet. We provided a thorough description of the generation of entropy during the flow of immiscible fluids through a porous saturated channel under the influence of radiative heat transfer, magnetic field and mass transfer. The considered problem's differential equations are analytically solved using the traditional method, and the results include a mathematical expression for the temperature profile, concentration distribution and flow fields of immiscible fluids. Graphs are used to illustrate the effects of various emerging parameters on the Bejan number profile, concentration distribution, thermal profile, entropy production number and flow characteristics. The emerging parameters include Soret number, Schmidt number, permeability parameter, couple stress parameter and Hartmann number. The study of Schmidt number, which is the ratio of momentum diffusivity and mass diffusivity, provides the information that how the diffusion of fluid particles affects the entropy generation. The range of these emerging design parameters can be helpful from an engineering perspective for those looking to create more efficient thermal systems. This study of entropy formation of immiscible fluids flowing via a channel has numerous practical applications that are used in thermal fusion reactors, cooling systems, petroleum products, etc. The solutions found for the subject under consideration can be applied to the cooling of thermal power plants, nuclear reactors, aircraft and more. Therefore, the entropy study offers prior knowledge for raising system efficiency, improving system design and optimizing system operating conditions. In presence of this framework, the current discussion offers the finest outcomes for the minimization of entropy

formation by examining the impact of numerous thermal and flow parameters. The evaluation of entropy production is carried out using the second law of thermodynamics. The impact of radiative heat exchange, mass exchange, porous medium and magnetic field on various flow variables has been discussed. The major findings of this research work are outlined as

- (1) The porous material reduces the friction-related heat dissipation in the porous saturation channel and also suppresses frictional dissipation. This is a crucial use for thermal engineering machinery.
- (2) The temperature profile, entropy production number and flow velocity enhance on increasing the couple stress parameter.
- (3) Hartmann number can be utilized to decrease the flow distribution, convective heat transfer and entropy production within the flow medium.
- (4) The production of entropy and temperature profile of immiscible fluid are reduced on enhancing the radiation parameter.
- (5) Permeability parameter reduces the flow velocity, production of entropy and thermal characteristics of immiscible couple stress fluid.
- (6) An important conclusion that arises from this study is that the extremum value of entropy production is achieved in lower porous region of the duct, however thermal characteristics achieved its extremum value in upper porous region.
- (7) The generation of entropy gets increased on enhancing the viscous dissipation parameter.
- (8) The concentration profile of immiscible nature of couple stress fluid diminishes with the ascending values of Schmidt number and Soret number.
- (9) Increasing values of Soret number and Schmidt number enhance the entropy production of immiscible type of couple stress fluid in a porous saturated duct.
- (10) The distribution of Bejan number reduces with the ascending values of Schmidt number and Soret number.
- (11) The result of viscous Newtonian fluids can be obtained in this study as a special case when $\eta \rightarrow 0$.
- (12) At the center of the channel, Bejan number is the maximum. This indicates a greater amount of workable energy and a lesser degree of irreversibility.
- (13) As compared to Region-1, Region-2's rate of entropy formation is higher close to the plate. This might be because the fluid in Region-2 is more viscous. This shows that entropy production increases as fluid viscosity increases.
- (14) The formation of entropy is maximum close to the wall surface in both the region in contrast to channel's midpoint. This shows that the frictional forces are predominant close to the wall surface and these forces increase the production of entropy. In contrast, Bejan numbers have greatest values close to the interface and minimum values close to the plates.

Appendix A

Flow velocity of couple stress fluid in Region-1 of the conduit:

$$u_1(y) = e^{-\alpha y} c_1 + e^{\alpha y} c_2 + e^{-\beta y} c_3 + e^{\beta y} c_4 - (PRes_1)/A_2 s_1. \quad (\text{A.1})$$

Temperature distribution in Region-1 of the conduit:

$$\begin{aligned} \theta_1(y) = & Br_1(Da^2 y^2 c_1 c_2 + 8e^{-y(\alpha+\beta)}(\alpha + \beta)_1^2 c_1 c_3 + 8e^{y(\alpha+\beta)} c_1 c_3(\alpha - \beta)_1^2 c_2 c_3) \\ & + Br_1(8e^{y(-\alpha+\beta)} c_1 c_3(\alpha - \beta)_1^2 c_1 c_4 - 8\xi e^{y\alpha} \alpha_1^2 c_2 - 8e^{y(-\alpha+\beta)}(\alpha \\ & - \beta)_1^2 c_1 c_4 \phi) + Br_1(8e^{y(\alpha+\beta)} c_1 c_3(\alpha + \beta)_1^2 c_2 c_4 + 4Da^2 y^2 \beta^4 c_3 c_4 \\ & + 4Ha^2 y^2 \beta^4 c_3 c_4 - 8\xi e^{-y\alpha} \alpha_1^2 c_1) + Br_1(-8\xi e^{-y\beta} \beta_1^2 c_3 8e^{-y(\alpha+\beta)}(\alpha \\ & + \beta)_1^2 c_1 c_3 \chi - 8e^{y(\alpha-\beta)}(\alpha - \beta)_1^2 c_2 c_3 \phi) + Br_1(-8\xi e^{y\beta} \beta_1^2 c_4 + 8e^{y(\alpha+\beta)}(\alpha \\ & + \beta)_1^2 c_2 c_4 \chi + \eta_1 e^{2y\alpha} c_2^2 \alpha^2 + \tau e^{2y\beta} c_4^2 \beta^2) + 2y^2 Br_1(P^2 Re^2 + 2Da^2 c_1 c_2 \\ & - 2Da^2 \alpha^2 c_1 c_2 + 4Da^2 Ha^2 \lambda^2 c_1 c_2 - 2Ha^2 \lambda^2 \alpha^2 c_1 c_2) s_1 + 2y^2 Br_1(2Ha^4 \lambda^4 c_1 c_2 \\ & + 2Da^4 c_3 c_4 - 2Da^2 \beta^2 c_3 c_4 + 4Da^2 Ha^2 \lambda^2 c_3 c_4 - 2Ha^2 \beta^2 \lambda^2 c_3 c_4) s_1 \\ & + Br_1(4Ha^4 \lambda^4 c_3 c_4 y^2 s_1 + 2e^{-2y(\alpha+\beta)} \tau e^{2y\alpha} c_3^2 \beta^2 + 2e^{-2y(\alpha+\beta)} \eta_1 e^{2y\beta} c_1^2 \alpha^2) \\ & + c_5 + y c_6. \end{aligned} \quad (\text{A.2})$$

Concentration field in Region-1 of the channel:

$$\begin{aligned} n_1(y) = & c_7 + y c_8 + Br_3(4Da^2 y^2 \alpha^4 c_1 c_2 + 4Ha^2 \lambda^2 y^2 \alpha^4 c_1 c_2 + e^{2y\alpha} \alpha^2 A_2 c_2^2) \\ & + Br_3(8A_2(e^{-2y(2\alpha+\beta)+y(3\alpha+\beta)} \alpha^2 \beta^2 c_1 c_3(\alpha + \beta)_1^2 + e^{y(\alpha-\beta)} \alpha^2 \beta^2 c_2 c_3 \\ & \times (\alpha - \beta)_1^2)) + Br_3(8A_2(e^{y(-\alpha+\beta)} \alpha^2 \beta^2 c_1 c_4(\alpha - \beta)_1^2 + e^{y(\alpha+\beta)} \alpha^2 \beta^2 c_2 c_4 \\ & \times (\alpha + \beta)_1^2)) + Br_3(4A_2 \beta^4 c_3 c_4 + e^{2y\beta} \beta^2 (Da^2 + Ha^2 \lambda^2) c_4^2 - 8(Da^2 \\ & + Ha^2 \lambda^2) PRes_1 \alpha_1^2 (c_1 e^{-y\alpha} + c_2 e^{y\alpha})) + Br_3 A_2 s_1 (e^{2y\alpha} c_2^2 \alpha_1^2 \\ & \times (Da^2 + \alpha^2 + Ha^2 \lambda^2) - 8e^{-y\beta} PRec_3 \beta_1^2) + Br_3(8e^{-y(\alpha+\beta)} (Da^2 + \alpha\beta \\ & + Ha^2 \lambda^2) c_1 c_3(\alpha + \beta)_1^2 + 8e^{y(\alpha+\beta)} (Da^2 + \alpha\beta + Ha^2 \lambda^2) c_2 c_4(\alpha + \beta)_1^2) \\ & + Br_3 A_2 s_1 (8e^{\alpha-\beta} c_2 c_3(\alpha - \beta)_1^2 (-Da^2 + \alpha\beta - Ha^2 \lambda^2) - 8e^{y\beta} PRec_4 \beta_1^2) \\ & + 2y^2 Br_3(P^2 Re^2 + 2Da^4 c_1 c_2 - 2Da^2 \alpha^2 c_1 c_2 + 4Da^2 Ha^2 \lambda^2 c_1 c_2 \\ & - 2Ha^2 \alpha^2 \lambda^2 c_1 c_2 + 2Ha^4 \lambda^4 c_1 c_2) s_1 + 2y^2 Br_3(P^2 Re^2 + 2Da^4 c_1 c_2 \\ & - 2Da^2 \alpha^2 c_1 c_2 + 4Da^2 Ha^2 \lambda^2 c_3 c_4 - 2Ha^2 \beta^2 \lambda^2 c_3 c_4 - 2Da^2 \beta^2 c_3 c_4) s_1 \\ & + 2y^2 Br_3(-2Ha^2 \lambda^2 \beta^2 c_3 c_4 + 2Ha^4 \lambda^4 c_3 c_4 + 2Da^4 c_3 c_4) s_1 \\ & + Br_3 A_2 e^{-2y(2\alpha+\beta)} (-8e^{3y(\alpha+\beta)} (-Da^2 + \alpha\beta - Ha^2 \lambda^2) c_1 c_4 s_1 (\alpha - \beta)_1^2) \\ & + Br_3 A_2 e^{-2y(2\alpha+\beta)} (e^{4y\alpha} c_3^2 (\beta^4 + Da^2 s_1 + \beta^2 s_1 + Ha^2 \lambda^2 s_1) \beta_1^2) \\ & + Br_3 A_2 e^{-2y(2\alpha+\beta)} (e^{2y(\alpha+\beta)} (\alpha^4 c_1^2 + Da^2 c_1^2 s_1 + Ha^2 \lambda^2 c_1^2 s_1) \alpha_1^2) \\ & + Br_3 A_2 e^{-2y(2\alpha+\beta)} (+e^{4y(\alpha+\beta)} (Da^2 + \beta^2 + Ha^2 \lambda^2) c_4^2 s_1 \beta_1^2). \end{aligned} \quad (\text{A.3})$$

The flow distribution of couple stress fluid in Region-2 of the porous pipe:

$$u_2(y) = c_9 e^{-\gamma y} + c_{10} e^{\gamma y} + c_{11} e^{-\delta y} + c_{12} e^{\delta y} - (PRen_k)/A_1. \quad (\text{A.4})$$

Temperature distribution in Region-2 of the conduit:

$$\begin{aligned} \theta_2(y) = & c_{13} + yc_{14} - Br_2(-8e^{-\gamma y}c_7\gamma_1^2\omega - 8e^{\gamma y}c_8\omega\gamma_1^2 - 8e^{-\delta y}\omega c_9\delta_1^2 \\ & - 8e^{\delta y}\omega c_{10}\delta_1^2 + e^{2y\gamma}c_8^2\gamma_1^2\varepsilon) + Br_2(e^{2y\delta}c_{10}^2\delta_1^2\varrho + 8e^{y(\gamma+\delta)}c_8c_{10}(\gamma \\ & + \delta)_1^2\kappa + 2y^2Ha^2\delta^4\lambda^2c_9c_{10}n_K^2n_\mu n_\sigma) + 8Br_2(e^{y(\gamma-\delta)}c_8c_9(\gamma - \delta)_1^2\kappa \\ & + e^{y(-\gamma+\delta)}c_7c_{10}(\gamma - \delta)_1^2\kappa + e^{-y(\gamma+\delta)}c_7c_9(\gamma + \delta)_1^2\kappa) + Br_2y^2 \\ & \times (2Da^2\gamma^4c_7c_8n_Kn_\mu^2 + 2Da^2\delta^4c_9c_{10}n_Kn_\mu^2 + 2Ha^2\gamma^4\lambda^2c_7c_8n_K^2n_\mu n_\sigma) \\ & + Br_2y^2(-2Da^2\delta^2c_9c_{10}n_Kn_\mu^2s_2 + 4Da^2Ha^2\lambda^2c_7c_8n_Kn_\mu n_\sigma s_2 + 4Da^2 \\ & \times Ha^2\lambda^2c_9c_{10}n_Kn_\mu n_\sigma s_2) + 2Br_2y^2(-Ha^2\gamma^2\lambda^2c_7c_8n_K^2n_\mu n_\sigma s_2 \\ & - Ha^2\delta^2\lambda^2c_9c_{10}n_K^2n_\mu n_\sigma s_2 + Ha^4\lambda^4c_7c_8n_K^2n_\sigma^2s_2) + 2Br_2y^2 \\ & \times (Da^4c_7c_8n_\mu^2s_2 + e^{2y\gamma}\gamma c_7^2\varrho\delta_1e^{-2y(\gamma+\delta)}\gamma_1\delta_1) + P^2y^2Re^2n_K^2s_2Br_2 \\ & + Br_2y^2(-2Da^2\gamma^2c_7c_8n_Kn_\mu^2s_2 + 2Ha^4\lambda^4c_9c_{10}n_K^2n_\sigma^2s_2 + e^{-2y(\gamma+\delta)}\gamma_1\delta_1 \\ & \times (e^{2y\delta}\delta c_7^2\varepsilon\gamma_1)). \end{aligned} \tag{A.5}$$

Concentration distribution in Region-2 of the conduit:

$$\begin{aligned} n_2(y) = & c_{15} + yc_{16} - 8PReBr_4n_Ks_2A(e^{-y\gamma}c_9\gamma_1^2 + c_{10}e^{y\gamma}\gamma_1^2 + e^{-y\delta}\delta_1^2c_{11} \\ & + e^{y\delta}c_{12}\delta_1^2) + Br_4(8e^{y(\gamma-\delta)}c_{10}c_{11}A(Da^2n_\mu s_2 + n_K(\gamma\delta n_\mu(\gamma\delta - s_2) \\ & + Ha^2\lambda^2n_\sigma s_2))(\gamma - \delta)_1^2) + Br_4(e^{2y\gamma}c_{10}^2A(Da^2n_\mu s_2 + n_K(Ha^2\lambda^2n_\sigma s_2 \\ & + \gamma^2n_\mu(\gamma^2 + s_2)))\gamma_1^2) + Br_4(8e^{-y(\gamma+\delta)}c_9c_{11}A(Da^2n_\mu s_2 + n_K(Ha^2\lambda^2n_\sigma s_2 \\ & + \gamma\delta n_\mu(\gamma\delta + s_2)))(\gamma + \delta)_1^2) + Br_4(8e^{y(\gamma+\delta)}c_{10}c_{12}A(Da^2n_\mu s_2 \\ & + n_K(Ha^2\lambda^2n_\sigma s_2 + \gamma\delta n_\mu(\gamma\delta + s_2)))(\gamma + \delta)_1^2) + 2Br_4y^2(2Da^4 \\ & \times (c_9c_{10} + c_{11}c_{12})n_\mu^2s_2 + 2Da^2n_Kn_\mu(2Ha^2\lambda^2(c_9c_{10} + c_{11}c_{12})n_\sigma s_2)) \\ & + 2Br_4y^2(n_\mu(\gamma^4c_9c_{10} + \delta^4c_{11}c_{12} - (\gamma^2c_9c_{10} + \delta^2c_{11}c_{12})s_2)) \\ & + 2Br_4y^2(n_K^2(P^2Re^2 + 2Ha^4\lambda^4(c_9c_{10} + c_{11}c_{12})n_\sigma^2)s_2) \\ & + 2Br_4y^2(2Ha^2\lambda^2n_\mu n_\sigma(\gamma^4c_9c_{10} + \delta^4c_{11}c_{12} - (\gamma^2c_9c_{10} + \delta^2c_{11}c_{12})s_2)) \\ & + Br_4A_1(8e^{3y(\gamma+\delta)}c_9c_{12}(Da^2n_\mu s_2 + n_K(\gamma\delta n_\mu(\gamma\delta - s_2) + Ha^2\lambda^2n_\sigma s_2)) \\ & \times (\gamma - \delta)_1^2) + Br_4A_1(e^{2y(\gamma+\delta)}c_9^2(Da^2n_\mu s_2 + n_K(Ha^2\lambda^2n_\sigma s_2 \\ & + \gamma^2n_\mu(\gamma^2 + s_2)))\gamma_1^2) + Br_4A_1(e^{4y\gamma}c_{11}^2(Da^2n_\mu s_2 + n_K(Ha^2\lambda^2n_\sigma s_2 \\ & + \delta^2n_\mu(\delta^2 + s_2)))\delta_1^2) + Br_4A_1(e^{4y(\gamma+\delta)}c_{12}^2(Da^2n_\mu s_2 + n_K(Ha^2\lambda^2n_\sigma s_2 \\ & + \delta^2n_\mu(\delta^2 + s_2)))\delta_1^2), \end{aligned} \tag{A.6}$$

where

$$\alpha = \sqrt{s_1 - \sqrt{s_1(-4Da^2 - 4Ha^2\lambda^2 + s_1)}/\sqrt{2}}, \tag{A.7}$$

$$\beta = \sqrt{s_1 + \sqrt{s_1(-4Da^2 - 4Ha^2\lambda^2 + s_1)}/\sqrt{2}}, \tag{A.8}$$

$$\zeta = \alpha^2\beta^2(Da^2 + Ha^2\lambda^2), \quad \xi = PRes_1(Da^2 + Ha^2\lambda^2), \tag{A.9}$$

$$\chi = s_1(\text{Da}^2 + \text{Ha}^2\lambda^2)(\text{Da}^2 + \alpha\beta + \text{Ha}^2\lambda^2), \quad (\text{A.10})$$

$$\phi = s_1(\text{Da}^2 + \text{Ha}^2\lambda^2)(-\text{Da}^2 + \alpha\beta - \text{Ha}^2\lambda^2), \quad (\text{A.11})$$

$$\eta_1 = (\text{Da}^2 + \text{Ha}^2\lambda^2)(\alpha^4 + \text{Da}^2s_1 + \alpha^2s_1 + \text{Ha}^2\lambda^2s_1), \quad (\text{A.12})$$

$$\tau = (\text{Da}^2 + \text{Ha}^2\lambda^2)(\beta^4 + \text{Da}^2s_1 + \beta^2s_1 + \text{Ha}^2\lambda^2s_1), \quad (\alpha + \beta)_1 = 1/(\alpha + \beta), \quad (\text{A.13})$$

$$(\alpha - \beta)_1 = 1/(\alpha - \beta), \quad \omega = P\text{Ren}_Ks_2\gamma_1^2(\text{Da}^2n_\mu + \text{Ha}^2\lambda^2n_Kn_\sigma s_2), \quad (\text{A.14})$$

$$\text{Br}_1 = 3\text{Br}/(3 + 4Nr)(\text{Da}^2 + \text{Ha}^2\lambda^2)s_1, \quad \alpha_1 = 1/\alpha, \quad \beta_1 = 1/\beta, \quad (\text{A.15})$$

$$\gamma = \sqrt{\frac{s_2}{2} - \frac{1}{2}\sqrt{\frac{-4\text{Da}^2s_2}{n_K} - \frac{4\text{Ha}^2\lambda^2n_\sigma s_2}{n_\mu} + s_2^2}}, \quad (\text{A.16})$$

$$\delta = \sqrt{\frac{s_2}{2} + \frac{1}{2}\sqrt{\frac{-4\text{Da}^2s_2}{n_K} - \frac{4\text{Ha}^2\lambda^2n_\sigma s_2}{n_\mu} + s_2^2}}, \quad (\text{A.17})$$

$$\varepsilon = (\text{Da}^2n_\mu + \text{Ha}^2\lambda^2n_Kn_\sigma)(\gamma^4n_Kn_\mu + \text{Da}^2n_\mu s_2 + \gamma^2n_Kn_\mu s_2 + \text{Ha}^2\lambda^2n_Kn_\sigma s_2), \quad (\text{A.18})$$

$$\varrho = (\text{Da}^2n_\mu + \text{Ha}^2\lambda^2n_Kn_\sigma)(\delta^4n_Kn_\mu + \text{Da}^2n_\mu s_2 + \delta^2n_Kn_\mu s_2 + \text{Ha}^2\lambda^2n_Kn_\sigma s_2), \quad (\text{A.19})$$

$$\kappa = (\text{Da}^2n_\mu + \text{Ha}^2\lambda^2n_Kn_\sigma)(\gamma^2\delta^2n_Kn_\mu + \text{Da}^2n_\mu s_2 - \gamma\delta n_Kn_\mu s_2 + \text{Ha}^2\lambda^2n_Kn_\sigma s_2), \quad (\text{A.20})$$

$$\gamma_1 = 1/\gamma, \quad (\gamma - \delta)_1 = 1/(\gamma - \delta), \quad \delta_1 = 1/\delta, \quad (\text{A.21})$$

$$\text{Br}_2 = 3\text{Br}/(4(4Nr + 3\bar{n}_k)n_k(\text{Da}^2n_\mu + \text{Ha}^2\lambda^2n_Kn_\sigma s_2)), \quad (\gamma + \delta)_1 = 1/(\gamma + \delta), \quad (\text{A.22})$$

$$\text{Br}_3 = \frac{3\text{Br Sc Sr}}{4(3 + 4Nr)(\text{Da}^2 + \text{Ha}^2\lambda^2)s_1}, \quad (\text{A.23})$$

$$\text{Br}_4 = \frac{3\text{Br Sc Sr}}{4(3\bar{n}_k + 4Nr)n_K(\text{Da}^2n_\mu + \text{Ha}^2\lambda^2n_Kn_\sigma s_2)}, \quad (\text{A.24})$$

$$A_1 = (\text{Da}^2n_\mu + \text{Ha}^2\lambda^2n_Kn_\sigma), \quad (\text{A.25})$$

$$A_2 = (\text{Da}^2 + \text{Ha}^2\lambda^2). \quad (\text{A.26})$$

References

1. S. O. Adesanya and O. D. Makinde, *Z. Nat. Forsch. A* **67**, 647 (2012).
2. Z. Abbas, J. Hasnain and M. Sajid, *Z. Nat. Forsch. A* **69**, 553 (2014).
3. K. Ramesh, *J. Mol. Liq.* **219**, 256 (2016).
4. J. Umavathi *et al.*, *Can. J. Phys.* **83**, 705 (2005).

5. F. Kamisli and H. F. Öztop, *Heat Mass Transf.* **44**, 751 (2008).
6. R. N. Kumar *et al.*, *Proc. Inst. Mech. Eng. E, J. Process Mech. Eng.* **235**, 1479 (2021).
7. R. N. Kumar *et al.*, *Phys. Scr.* **96**, 1 (2021).
8. R. N. Kumar *et al.*, *Int. J. Mod. Phys. B* **36**, 2250170 (2022).
9. K. K. Asogwa *et al.*, *Int. Commun. Heat Mass Transf.* **131**, 1 (2022).
10. M. Ravisha *et al.*, *Int. J. Mod. Phys. B* **37**, 2350020 (2022).
11. S. I. Abdelsalam and A. Z. Zaher, *Math. Model. Nat. Phenom.* **17**, 1 (2022).
12. A. M. Alsharif *et al.*, *Appl. Math. Mech.* **43**, 931 (2022).
13. S. I. Abdelsalam, K. S. Mekheimer and A. Z. Zaher, *Waves Random Complex Media* **1** (2022).
14. T. Thumma *et al.*, *Appl. Math. Comput.* **421**, 1 (2022).
15. V. K. Stokes, Couple stresses in fluids in theories of fluids with microstructure, *Theories of Fluids with Microstructure: An Introduction* (Springer, 1984), pp. 34–80.
16. V. K. Stokes, *Theories of Fluids with Microstructure: An Introduction* (Springer, 2012).
17. T. Ariman and A. S. Cakmak, *Phys. Fluids* **10**, 2497 (1967).
18. K. S. Mekheimer, *Biorheology* **39**, 755 (2002).
19. D. Srinivasacharya, N. Srinivasacharyulu and O. Odelu, *Int. Commun. Heat Mass Transf.* **36**, 180 (2009).
20. M. N. Khan *et al.*, *Int. J. Mod. Phys. B* **36**, 2250187 (2022).
21. R. Raza, R. Naz and S. I. Abdelsalam, *Numer. Methods Partial Differ. Equ.* **39**, 975 (2022).
22. A. Bejan, *J. Appl. Phys.* **79**, 1191 (1996).
23. A. Bejan, G. Tsatsaronis and M. Moran, *Thermal Design and Optimization* (John Wiley and Sons, New York, 1996).
24. A. Bejan, *J. Heat Transf.* **101**, 718 (1979).
25. A. Bejan, *Energy* **5**, 720 (1980).
26. V. Sridhar *et al.*, *Waves Random Complex Media* **1** (2022).
27. M. Faizan *et al.*, *Mathematics* **10**, 3157 (2022).
28. O. D. Makinde and A. S. Eegunjobi, *Entropy* **15**, 4589 (2013).
29. J. Srinivas, J. R. Murthy and K. S. Sai, *Comput. Therm. Sci., Int. J.* **7**, 123 (2015).
30. G. Nagaraju *et al.*, *Heat Transf.-Asian Res.* **46**, 316 (2017).
31. Y. Aksoy, *Int. J. Thermal Sci.* **107**, 1 (2016).
32. S. O. Adesanya *et al.*, *Energy* **93**, 1239 (2015).
33. J. Srinivas, J. V. Murthy and O. A. Bg, *J. Braz. Soc. Mech. Sci. Eng.* **39**, 2191 (2017).
34. J. R. Murthy and J. Srinivas, *Heat Transf.-Asian Res.* **44**, 468 (2015).
35. S. Jangili *et al.*, *Int. J. Appl. Comput. Math.* **3**, 3759 (2017).
36. V. S. Arpaci, *AIAA J.* **24**, 1859 (1986).
37. V. S. Arpaci, *Int. J. Heat Mass Transf.* **30**, 2115 (1987).
38. P. K. Yadav and A. Kumar, *Int. Commun. Heat Mass Transf.* **124**, 1 (2021).
39. P. K. Yadav *et al.*, *Waves Random Complex Media*, 1 (2022).
40. P. K. Yadav, A. Kumar and A. N. Filippov, *Colloid J.* **85**, 1 (2023) (accepted).
41. W. Jamshed *et al.*, *Phys. Scr.* **96**, 064006 (2021).
42. A. Alhadhrami *et al.*, *Case Stud. Therm. Eng.* **28**, 101483 (2021).
43. M. Al-Maliki, K. Al-Farhany and I. E. Sarris, *Symmetry* **14**, 2181 (2022).
44. I. E. Sarris, I. Lekakis and N. S. Vlachos, *Int. J. Heat Mass Transf.* **47**, 14 (2004).
45. R. R. Gold, *J. Fluid Mech.* **13**, 505 (1962).
46. H. Darcy, *Les Fontaines Publiques de La Ville de Dijon* (Victor Dalmont, 1856).
47. D. Y. Khanukaeva *et al.*, *Eur. J. Mech. B, Fluids* **76**, 73 (2019).
48. O. Ojjela and N. N. Kumar, MHD heat and mass transfer of couple stress fluid through porous medium between two parallel plates with chemical reaction, hall and ion slip

- effects and the conference is held on BESU shibpur, *Proc. 58th Congress of ISTAM* (Howrah, W.B., India, 2013), p. 1.
49. E. M. Sparrow, *Radiation Heat Transfer*, Augmented Edition (Routledge, New York, 2018).
 50. M. Q. Brewster, *Thermal Radiative Transfer and Properties* (John Wiley and Sons, 1992).
 51. A. S. Butt *et al.*, *Phys. Scr.* **85**, 035008 (2012).
 52. S. Kalyan, A. Sharan and A. J. Chamkha, *J. Heat Transf.* **52**, 267 (2013).
 53. A. Bejan, *Convection Heat Transfer* (John Wiley and Sons, 2013).
 54. S. Paoletti, F. Rispoli and E. Sciubba, *ASME AES* **10**, 21 (1989).
 55. J. R. Murthy and J. Srinivas, *Int. J. Heat Mass Transf.* **65**, 254 (2013).
 56. P. K. Yadav and A. K. Verma, *Eur. Phys. J. Plus* **135**, 1 (2020).
 57. S. O. Adesanya and O. D. Makinde, *Comput. Appl. Math.* **34**, 293 (2015).
 58. S. Chikh *et al.*, *Int. J. Heat Mass Transf.* **38**, 1543 (1995).
 59. R. Ellahi, M. M. Bhatti and K. Vafai, *Int. J. Heat Mass Transf.* **71**, 706 (2014).
 60. T. Zhao *et al.*, *Appl. Math. Mech.* **42**, 1205 (2021).
 61. H. M. Meisam, *J. Mech. Eng. Autom.* **5**, 26 (2015).
 62. J. C. Umavathi, J. P. Kumar and A. J. Chamkha, *Turk. J. Eng. Environ. Sci.* **33**, 221 (2009).